

# Inorganic Materials for Archival Holographic Recording

V. Weiss\*, A. A. Friesem, and A. Peled†

*The Weizmann Institute of Science, Physics of Complex Systems, Rehovot, 76100 Israel*

Inorganic material systems for archival holographic recording are considered. The emphasis is on bleached silver halide emulsions and CdS and Se colloidal solutions. The bleached silver halide emulsions were investigated to determine the salient parameters that influence photolytic stability and diffraction efficiency. The experimental and theoretical investigations reveal that the silver halide grains, the gelatin matrix, and the gelatin matrix voids are contributing to the holographic storage mechanism. By the adsorption of bromine from the processing solutions on the silver halide grains, it is possible to extend the photolytic stability almost indefinitely. By suppressing the influence of the gelatin matrix and the gelatin matrix voids by chemical processing, it is possible to obtain increased diffraction efficiencies reaching 70%. The colloidal solutions were investigated to determine the basic mechanisms for photodepositing ultrathin surface relief holographic gratings. The results reveal that the photodeposition includes primary photoreduction and secondary adsorption controlled processes. A model is developed to predict the spatial frequency response of the colloidal solutions showing that the recorded spatial resolution is limited by the particle sizes.

Journal of Imaging Science and Technology 41: 355–371 (1997)

## Introduction

During the past three decades, a multitude of materials were investigated for holographic recording.<sup>1–5</sup> These included materials for thin, thick, absorptive, and phase holograms that were evaluated for a variety of possible applications. Certain materials and processes are advantageous because of either their high exposure sensitivity, high diffraction efficiency (DE), high signal-to-noise ratio (SNR), good archival storage stability, or real-time recording capability. Yet none of the materials exhibit simultaneously all of the advantages.<sup>1–5</sup> For example, absorptive materials, such as silver halide (AgHal) emulsions, have relatively high exposure sensitivity and good archival storage stability, but only low DE. Dichromated gelatin materials have high DE and excellent noise characteristics, but relatively poor exposure sensitivities and environmental stability. Photopolymers have relatively high DE and SNR, and real-time recording capability, but relatively poor exposure sensitivity, and photochromic materials have real-time recording and erasure capability, but only low DE and exposure sensitivity.<sup>1–5,6</sup>

In this article, we describe the investigations conducted at the Weizmann Institute of Science during the last 10 years with the purpose of improving existing materials and developing new ones for holographic recording. Specifically, we consider inorganic optical recording systems with focus on bleached silver halide (AgHal) emulsions,<sup>7–10</sup> which are undoubtedly the most common materials for holographic

recording. In addition, we consider inorganic colloids, that photodeposit thin films on substrates when illuminated with laser radiation.<sup>11–15</sup> With these it is possible to record ultrathin holographic gratings of very high resolution.

The photochemical and photophysical processes are investigated for elucidating the basic recording and storage mechanisms with these materials. An analysis of holographic recording and readout shows certain advantages over conventional optical recording or spectroscopy.<sup>16,17</sup> An important advantage is that, in addition to detecting changes in absorption as in spectroscopy holography can also detect dispersive changes; these dispersive changes are most important in holographic phase materials where the image is stored by refractive index modulations. With AgHal phase holograms, refractive index modulations are obtained by chemically bleaching the developed silver image so that relatively high diffraction efficiencies are obtained. In our experimental and theoretical studies, we found several factors that contribute to the refractive index modulations and that it is possible to differentiate between individual contributions.<sup>7–10</sup> Parameters that influence these individual contributions are altered to improve the overall holographic performance.

Selenium colloids and recently developed cadmium sulfide (CdS) colloids are investigated to determine the basic mechanisms of photodeposition.<sup>14</sup> In addition, an analysis of the frequency response of holographic ultrathin surface relief gratings is developed in which the colloid particle size is related to the resolution capabilities.<sup>12,13</sup>

## Recording and Readout Principles

**Photochemical Recording.** To record optical information in any material, photons must be absorbed by that material and cause chemical changes. These are primary photochemical reactions and can be described by the first and second laws of photochemistry.<sup>18</sup> In certain recording materials, the primary reactions are followed by secondary reactions. These may either occur in situ as in

Original manuscript received March 7, 1996.

\* V. Weiss is also affiliated with ELOP Electrooptics Industries, Kiryat Weizmann, Rehovot, 76111 Israel, e-mail: feweiss@weizmann.weizmann.ac.il

† A. Peled is also affiliated with CTEH (aff. Tel Aviv University), Holon, Israel 58102

©1997, IS&T—The Society for Imaging Science and Technology

photopolymerization or they may be induced in vitro by reaction with so-called developers as in photoresists and silver halide emulsions. The amplification of primary reactions as achieved by secondary reactions can be most significant. For example, in photopolymerization the amplification may reach 5 orders of magnitude,<sup>19</sup> and with chemical development of AgHal emulsions it may extend from 6 to 9 orders of magnitude.<sup>19,20</sup>

Quantum yield improvement by increasing the absorption cross section, improving the photochemical conversion, or minimizing relaxation and side reactions is generally termed sensitization. Therefore, by sensitizing the primary process and/or by enhancing the secondary amplification step, improvements in exposure sensitivity can be achieved.

Let us illustrate photochemical recording by considering the most simple one-step primary photochemical reaction, represented by



We assume that  $A$  is irreversibly converted to  $B$ , and that thermal contributions can be neglected. In this case, the differential rate equations, describing the concentration change of  $A$  and  $B$  with time, are given by

$$-dA/dt = \xi A = dB/dt, \quad (2)$$

where  $\xi$  is the overall photochemical reaction rate constant, which is given by

$$\xi = 2.303 I_A \varepsilon_A \phi_A (\lambda_A / Nhc), \quad (3)$$

where  $I_A$  is the light intensity (in joules  $\text{cm}^{-2} \text{sec}^{-1}$ ) at wavelength  $\lambda_A$ ,  $\varepsilon_A$  the decadic molar absorption coefficient [or cross section in  $\text{cm}^2/\text{mol}$ ],  $\phi_A$  the quantum yield,  $N$  Avogadro's number,  $h$  Planck's constant, and  $c$  the speed of light. Integrating Eq. 2 yields

$$A(t, E) = A_0 \exp[-\xi t] = A_0 \exp[-\xi' E] \quad (4a)$$

$$B(t, E) = A_0 \{1 - \exp[-\xi t]\} = A_0 \{1 - \exp[-\xi' E]\}, \quad (4b)$$

where  $A_0$  is the initial concentration of  $A$ ,  $\xi'$  is the intensity independent rate constant, and  $E$  is the exposure given by the intensity multiplied by the exposure time, i.e.,  $E = It$ . In special cases, where the primary reactions are reversible as with photochromic materials,<sup>21,22</sup> it is possible to exploit real-time recording and erasure.<sup>6,23</sup>

**Storage and Read-out Mechanisms.** Most mechanisms of inducing refractive index changes can well be explained by the Lorentz-Lorenz relation.<sup>24</sup> For an ideal multicomponent system where the electronic interactions between the components and the matrix may be neglected, it is necessary to consider the individual contributions from each component  $i$  so that<sup>24</sup>

$$\frac{n^2 - 1}{n^2 + 2} = \sum_i \frac{\rho_i R_i}{M_i}, \quad (5)$$

where  $\rho_i$  is the material density;  $R_i$  is the molar refraction given by  $R_i = 4\pi N \alpha_i / 3M_i$ , with  $\alpha_i$  the molecular polarizability; and  $M_i$  is the molecular weight.

Equation (5) indicates that the refractive index may be affected by three basic mechanisms:

(1) Concentration changes shift the relative contributions of the individual components. To be effective, this requires

that a difference exists in the refractive properties among the components; (2) the molar refraction  $R_i$  of one or more components is changed. The molar refraction can be influenced by the dispersive (real) contribution of strong absorption bands as described by the Kramers-Kronig relations<sup>16,23</sup> and/or be induced by changes in molecular polarizability, which originates from changes in molecular structure; and (3) the density  $\rho_i$  of one or more of the components is changed. This requires an important change in the sterical conformation of the molecules or material transport effects. For the specific case of the one-step reaction as described by Eq. 1, the exposure-dependent refractive index change can be written as

$$\Delta n(E) = R_0 A_0 \Delta R \{1 - \exp[-\xi' E]\}, \quad (6)$$

where  $R_0$  is a constant approximately given by  $R_0 = (n^2 + 2)^2 / 6n$ , and  $\Delta R$  is the change in molar refraction between  $A$  and  $B$  given by  $\Delta R = R_B - R_A$ .<sup>23,24,25</sup>

So far it has been assumed that the above three mechanisms only affect local changes in concentration, molar refraction and/or density of reactants and products, induced by primary photochemical reactions. However, if the primary reactions are followed by secondary ones, then major influences on the matrix can take place so that the above mechanisms and their assumptions are no longer valid. Examples for such behavior are photopolymerization and chemical processing of photocrosslinked gelatin for which significant density changes in the polymeric matrix are known to occur.<sup>5,6,24</sup> Nevertheless, as shown below, this difficulty can be overcome by considering the matrix as an additional active component.

**Holographic Recording and Readout.** For the study of photochemical and photophysical processes in recording materials, linear holographic gratings are most convenient. Typical holographic recording and readout configurations are schematically depicted in Fig. 1. For holographic recording as shown in Fig. 1(a) a laser beam is split into two beams that are then expanded and collimated. One serves as the reference beam with intensity  $I_R$  and the other as the object beam with intensity  $I_O$ . When these two plane waves interfere at the recording plane, the intensity  $I(x)$  of the interference pattern can be written as

$$I(x) = (I_R + I_O)[1 + V \cos(2\pi x/d)], \quad (7)$$

where  $V = 2(I_O I_R)^{1/2} / (I_R + I_O)$  is the fringe visibility (or fringe contrast) and  $d$  is the fringe spacing given by Bragg's equation  $d = \lambda / [2 \sin \theta]$ , with  $\lambda$  being the wavelength of the laser and  $\theta$  the angle of incidence. The reciprocal value of the fringe spacing determines the spatial frequency  $f$  as

$$f = 1/d = 2 \sin \theta / \lambda, \quad (8)$$

which shows that for a given wavelength,  $f$  can be increased by increasing the incidence angle.

Recording the interference pattern according to Eq. 7 in a photosensitive material results in a grating having a spatial modulation of either the absorption coefficient  $a(x)$ , or the refractive index,  $n(x)$  in the form of

$$a(x) = a_0 + a_1 \cos(2\pi x/d), \quad (9a)$$

$$n(x) = n_0 + n_1 \cos(2\pi x/d), \quad (9b)$$

where  $a_0$  denotes the average value of the absorption coefficient,  $n_0$  the average refractive index,  $a_1$  the modulation

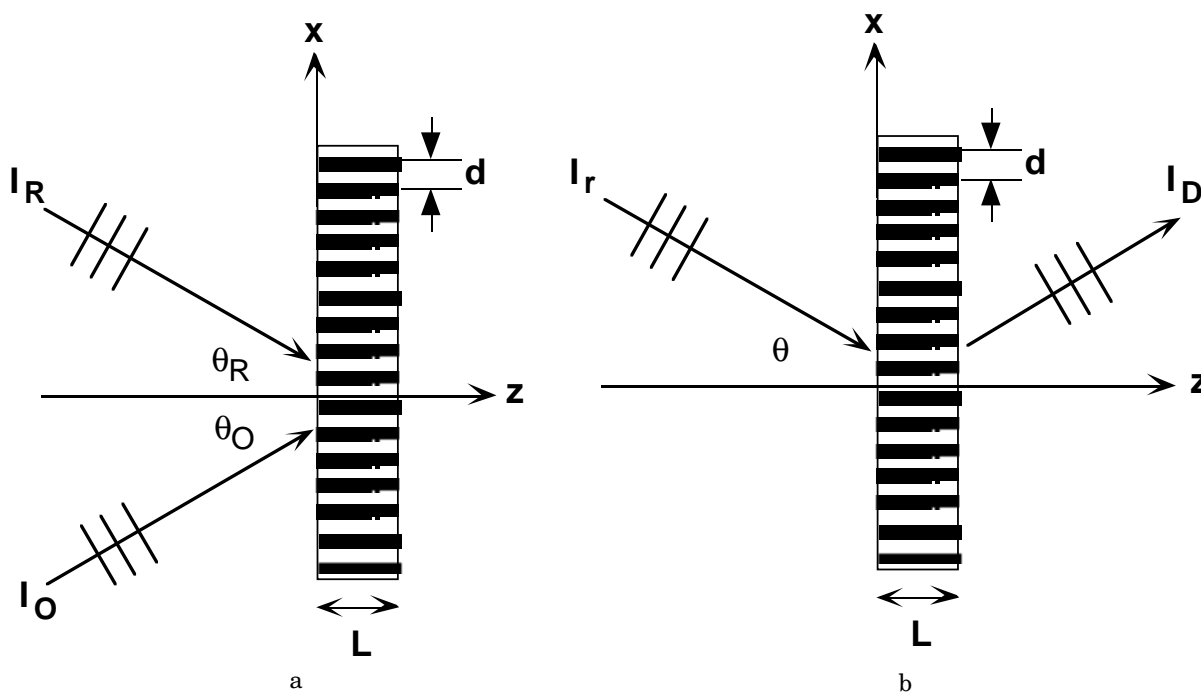


Figure 1. Holographic recording and readout configurations: (a) recording; (b) readout.

amplitude of the absorption coefficient, and  $n_1$  the modulation amplitude of the refractive index. Equation 9 is valid under the assumption of a linear response of absorption and refraction as a function of exposure in which case higher order terms can be neglected. While this may not be true for the complete exposure response region, usually in most recording media a sufficiently large linear exposure region exists.<sup>1</sup>

The readout of the recorded holographic gratings [Fig. 1(b)] determines the diffraction efficiency (DE), which is defined as the ratio of the first order diffracted to the incident light powers. When the thickness  $L$  of the recording layer is more than 1 order of magnitude larger than the grating period  $d$ , then the coupled wave theory for thick gratings can be applied.<sup>26</sup> The diffraction efficiency as a function of exposure  $\eta(E)$  can then be written as:<sup>23,26</sup>

$$\eta(E) \propto \sin^2 \left( \frac{\pi n_1 \{B_1(E)\} L}{\lambda \cos \theta} \right) + \sinh^2 \left( \frac{a_1 \{B_1(E)\} L}{2 \cos \theta} \right), \quad (10)$$

where  $\lambda$  and  $\theta$  are the wavelength and the incidence angle of the readout beam, respectively, and  $B_1(E)$  is the exposure-dependent amplitude of the spatial concentration modulation of the photochemical product  $B$  (see Eq. 1). The first and second terms in Eq. 10 represent the phase and amplitude contributions, respectively. The higher the amplitude term, the larger the losses in the grating. Consequently, high diffraction efficiency will only be obtained by reducing the amplitude term, reaching a theoretical  $\eta$  of 100%, for a completely lossless phase grating ( $a_0 = a_1 = 0$ ).<sup>26</sup>

Holography can also be exploited for the investigation of basic photochemical/photophysical processes in solid matrices, because it has certain advantages over either conventional optical recording or absorption spectroscopy.<sup>17,27,28</sup> The first and probably most important advantage of holography is its sensitivity to changes of both

absorption as well as refractive index. In particular, the refractive index changes can be probed at wavelengths outside the absorption band where the recorded information is not destroyed when probed with a high intensity beam, leading to improved detection sensitivity. Other dispersion-sensitive methods, such as optical rotatory spectroscopy and ellipsometry, are limited to either optically active materials or ultrathin layers and cannot be used for real-time investigations. In this article, we show that the dispersive properties of holographic phase gratings recorded in photographic AgHal emulsions can yield important information about conformational changes in macromolecular matrices that with other methods could not have been obtained in a conclusive manner.

Second, with holographic recording, the light-induced changes are probed directly without background by monitoring the DE; consequently, refractive index changes of  $10^{-7}$  or absorption changes of  $10^{-5}$  can still be detected.<sup>27</sup> With conventional spectroscopy, in contrast, the measured optical density data also contains background from nonreactive species and optical noise, which increases the experimental error; typical detection limits in absorption spectroscopy would be  $10^{-3}$ . Furthermore, with holographic recording at very low exposures, the square of the concentration changes and the rate constants is probed,<sup>16,17</sup> resulting in significantly higher sensitivity especially during the initial phases of the photoinduced processes.<sup>6</sup> In comparison with either conventional direct optical recording or spectroscopy, the optical density, which is linearly dependent on concentration, is detected.

Third, holographic recording can be exploited for accurately determining the resolution capabilities of the recording materials and investigating their microscopic characteristics<sup>12,13</sup> as shown in this article. The spatial frequency of the recorded holographic gratings can be easily varied by changing the incidence angles of the recording beams. This is more advantageous than methods using optical resolution charts that introduce unwanted optical

noise such as diffraction and speckles. In addition, in holography only very small sample areas are needed, because the measured changes occur on microscopic scale (around the wavelength of the readout light); for example, an area of 50  $\mu\text{m}$  may typically record 25 to 100 fringes of the holographic interference pattern, which is sufficient to cause diffraction.

**Material Parameters.** Before dealing with specific recording materials and processes, let us consider some relevant parameters for holographic recording and readout.

1. Resolution is related to the spatial frequency [lines/mm] that can be recorded. Resolution is conveniently determined by measuring the spatial frequency response of the recording medium, i.e., the dependence of the diffraction efficiency (DE) on spatial frequency from which the modulation transfer function (MTF) is derived.<sup>20,29</sup> The MTF is characteristic of the microscopic recording mechanism and is related to the size of the recording unit (pixel). As a rule, the minimal linewidth that can be resolved in a given recording material (without deterioration in readout) is about 1 order of magnitude larger than the pixel size.
2. Exposure sensitivity is related to the exposure needed to obtain a predetermined value of the measured readout parameter. In our investigations, the holographic exposure sensitivity is defined as the exposure value in radiometric units [ $\text{J cm}^{-2}$ ] needed to obtain maximal DE ( $\text{DE}_{\text{max}}$ ). For direct optical recording, the exposure sensitivity is defined as the exposure needed to obtain 50% of the maximal OD ( $\text{OD}_{\text{max}}$ ). A deviation in exposure sensitivity as a result of varied intensity and exposure time for a given exposure value is known as<sup>20</sup> the reciprocity failure (RF).
3. Spectral sensitivity is defined as the exposure sensitivity at a given wavelength. Consequently, the use-

ful wavelength range in which the material can record optical radiation can be related to as the spectral response region. The broader the spectral response region, the wider the choice of light sources that can be used with the same recording material.

4. Signal-to-noise ratio (SNR) is related to readout parameters such as image contrast. The ratio of the maximal signal intensity to the background intensity in the output image is a measure of SNR.<sup>2,5</sup> Factors that may reduce SNR are structural inhomogeneities in recording material, that lead to light scattering.<sup>2,5</sup>
5. Dynamic Range and Exposure Latitude determine the degree of freedom of the exposure conditions during recording and influence the optical performance.<sup>2</sup> The dynamic range is the total change in absorbance or refractive index that can be obtained and the exposure latitude is the exposure range in which a required change in absorbance or refractive index is achieved. A limited dynamic range could limit the maximal DE.<sup>10,23</sup>
6. Storage stability is determined by how readout light, background and thermal radiation, and other environmental factors affect the readout performance of the recording material as a function of time.

A variety of materials for optical holographic recording have been investigated.<sup>1-5</sup> The important materials together with their recording mechanisms, chemical processing, and relevant parameters are listed in Tables I and II. In this article, we shall consider in detail bleached silver halide (AgHal) emulsions and inorganic colloids.

### Silver Halide Emulsions

#### Recording, Processing, and Readout Mechanisms.

Optical recording in AgHal emulsions involves two steps. In the primary recording step, a latent image is formed

**TABLE I. Recording Mechanism, Processing and Recording Parameters of Optical Recording Materials**

Recording materials	Recording mechanism	Chemical processing	Sensitivity ( $\text{mJ/cm}^2$ )	Spectral response (nm)
AgHal emulsion				
• conventional	photoredox	• develop, fix	$10^{-4}$ to $10^{-1}$	250 to 700
• bleached	photoredox	• develop, bleach	$10^{-2}$ to 1	250 to 700
Dichromated gelatin (DCG)	photoredox, x-link	develop, fix, dehydrate	10 to $10^3$	350 to 580
Photoresist	photoredox, x-link	fix	10 to $10^3$	300 to 500
• negative	photoredox	fix		
• positive				
Photopolymer	photoredox, polymerization	none	1 to $10^3$	300 to 650
Photochromics	color center or organic dyes	none	$10^2$ to $\geq 10^3$	300 to 700
Photothermo-plastics	photocharge, electrostatic/thermal deformation	none	$10^{-2}$ to $10^{-1}$	400 to 650
Photorefractive ( $\text{Bi}_{12}\text{Si}_2\text{O}_{20}$ )	photocharge, electrooptic	none	$10^{-1}$ to $\geq 10^2$	350 to 550
Inorganic colloids (a-Se)	photoredox/photodeposition	none	$10^3$ to $\geq 10^4$	250 to 550

**TABLE II. Read-Out Parameters of Optical Recording Materials**

Recording materials	Modulation	DE	Resolution (lines/mm)	SNR	Erasable
AgHal emulsion	amplitude/phase	$0.05 \leq 0.70$	$\leq 10^4 \leq 10^4$	$> 100 \approx 50$	no
DCG	phase	$\geq 0.90$	$\geq 10^4$	$\approx 1000$	no
Photoresist	phase	0.70	$> 10^3$	$\approx 50$	no
Photopolymer	phase	$\geq 0.90$	$> 10^3$	$> 100$	no
Photochromics	amplitude	0.04	$\leq 10^4$	$> 100$	yes, light, heat
Photothermo-plastics	phase	0.30	$\leq 10^3$	$\approx 50$	yes, heat
Photorefractive	phase	0.25	$\geq 10^3$	$\approx 100$	yes, light, heat
Inorganic colloids (a-Se)	phase/amplitude	0.10	$\geq 10^3$	$\approx 50$	no

that needs a secondary, chemical amplification (development) step of the latent image.<sup>20,30-32</sup> The explanation for the mechanism of latent image formation in silver halide (AgHal) emulsions is still controversial.<sup>20,30-32</sup> The most widely accepted model was advanced by Gurney and Mott<sup>33</sup> about 50 years ago and was refined by others.<sup>20,30</sup> In this model, the latent image is viewed as consisting of small metallic silver specks created by a stepwise growth of electronic and ionic events. In other models, the silver specks are treated as a new phase nucleated from the supersaturated AgHal crystals.<sup>20,30</sup> All these models assume that the latent image silver specks catalyze the secondary development step. Yet the silver speck explanation cannot fully account for all photographic phenomena,<sup>31</sup> so a photoelectrochemical model (PEC) that treats the recording and amplification processes in a comprehensive manner was developed.<sup>31,32</sup> This PEC model assumes a monosize and monosensitive array of AgHal detectors having a given grain redox potential ( $E_g$ ). The potential  $E_g$ , which is influenced both by light and by chemical environment, is expressed as being proportional to the logarithm of the ratio of the number of photons over the number of oxidized defects in the grain. Chemical amplification is controlled by  $E_g$  through the induction period ( $\tau$ ) of chemical development.<sup>32</sup>

The secondary processing step in holographic recording usually includes additional stages.<sup>1-5</sup> First, conventional chemical development (amplification) of holographically recorded latent images converts the AgHal grains to elementary silver ( $\text{Ag}^0$ ) particles, resulting in an amplitude hologram with low diffraction efficiency (DE).<sup>1-5</sup> Then by oxidizing the holographic silver image with appropriate bleaching solutions, the  $\text{Ag}^0$  particles are reconverted into silver salt (usually silver bromide) grains, resulting in a phase hologram with much higher DE.<sup>1-5</sup> Before proceeding, let us first clarify the terminology used in chemical processing of bleached AgHal materials. We start by differentiating between processing procedures (a sequence of steps) and formulations (a list of chemicals). Below are the definitions for terms we use when dealing with chemical processing that involves bleaching.

Bleach procedures that result in a reversal (or complementary) image of the original record are referred to as *reversal bleach* (RB).<sup>2-5</sup> Analogously, procedures that result in a direct copy of the original record are referred to as *direct bleach*.<sup>3</sup> Finally, procedures that completely remove by bleaching and fixing all of the silver and silver halide from the emulsion are termed *silver halide sensitized gelatin* (SHSG).<sup>5,8,9</sup> Any bleach formulation that reduces and dissolves  $\text{Ag}^0$  particles and completely removes them from the emulsion layer during the bleaching step is a *solvent bleach*. Solvent bleach formulations can be used with RB and SHSG procedures.<sup>5,9</sup> Any bleach formulation that rehalogenates bleached silver during the bleaching step is a *rehalogenating bleach*. Rehalogenating bleach formulations can be used with direct bleach, RB, and SHSG procedures.<sup>7,8,9</sup>

Except for SHSG, the AgHal grains in bleached holograms, unfortunately, retain some light sensitivity and may darken photolytically by exposure to readout or environmental radiation. The techniques to overcome photolytic darkening can be divided into three groups: (1) recrystallization into less light-sensitive silver salts<sup>34</sup> such as ferrocyanides<sup>34,35</sup> and iodides<sup>34,36</sup>; (2) postprocessing with desensitizing dyes such as safranine derivatives<sup>37,38</sup>; and (3) desensitization by aqueous bromine<sup>3,39</sup> or halogen vapors.<sup>40,41</sup> Unfortunately, recrystallization according to (1) significantly increases scat-

tering<sup>34,35</sup>, dye desensitization according to (2) substantially complicates the chemical processing with the unpleasant side effect of irreversibly dyeing the holograms and the processing equipment<sup>3</sup>; and, halogen desensitization according to (3) also complicates processing and necessitates additional safety precautions such as fume hoods, due to toxic halogen vapors.<sup>3</sup>

To increase the photolytic stability of bleached holograms and to overcome the disadvantages of the above methods, new ammonium dichromate and ferric-sulfate-based bleach formulations were developed.<sup>7</sup> In these formulations, minute quantities of bromine are chemically synthesized in the bleach bath by chemical oxidation of bromide. These bleach formulations also simplify the processing procedures, because no clearing bath and post processing desensitization are needed and they increase the holograms' transmittance and the DE.<sup>7</sup> Unfortunately, the DE of holograms stored in bleached AgHal emulsions are limited to less than 70%,<sup>2-5,7,42,43</sup> so they do not reach the theoretical value of 100% approached by dichromated gelatins or photopolymers<sup>3-5,6</sup> (see Table II). The limitation in DE for bleached AgHal emulsions originates from several factors: (1) the AgHal grains grown in size by recrystallization in the bleach bath scatter the readout light and thereby reduce DE and SNR;<sup>2-5,7,42,43</sup> (2) emulsion thickness variations that result from material removal during chemical processing;<sup>44</sup> (3) nonlinear recording that result from nonlinear exposure responses;<sup>2-5,45,46</sup> (4) light scattering by AgHal grains during recording;<sup>46,47</sup> and (5) absorption losses from emulsion staining that result from developer/bleach interactions, sensitizer residues, and photolytic darkening.<sup>3,7,9,42,43</sup>

Another significant factor that may reduce DE depends on the limited dynamic range of refractive index modulation obtained with chemical processing. The dynamic range of refractive index modulation originates from the reactions of individual emulsion components with the chemical processing solutions.<sup>7-9</sup> To explain the origin of the individual contributions to the overall refractive index modulation in bleached AgHal emulsions, we present Fig. 2, which schematically depicts the principal recording and processing steps in bleached AgHal emulsions for the RB and SHSG processing procedures.

With RB processing procedures, shown in the upper part of Fig. 2 (Steps 1 and 2), the  $\text{Ag}^0$  particles in the exposed and developed areas are during the bleaching step either completely removed (with solvent bleach formulations) or transferred to the unexposed areas and reconverted to AgHal (with rehalogenating bleach formulations).<sup>43,48</sup> For comparison, note that with direct (or conventional) bleach processing,<sup>3-5</sup> the AgHal grains from the unexposed areas are first removed by fixing and then the remaining silver particles are reconverted into silver salt grains. With both the RB and direct bleach procedures, the primary contribution to the refractive index variation is due to the AgHal grains. Holographic patterns are stored as a spatial modulation in the number of AgHal grains imbedded in gelatin; such a spatial modulation will result in a refractive index modulation where those areas with AgHal grains have higher refractive indices than those without.

A secondary contribution originates from the gelatin binder. During the development and bleaching steps, reaction by-products are generated that in turn cause gelatin crosslinking so as to harden (tan) the gelatin matrix.<sup>20,49</sup> Such differential hardening is believed to result in additional refractive index modulation<sup>7,42,43,48,50</sup> where those regions with hardened gelatin have higher refractive indices

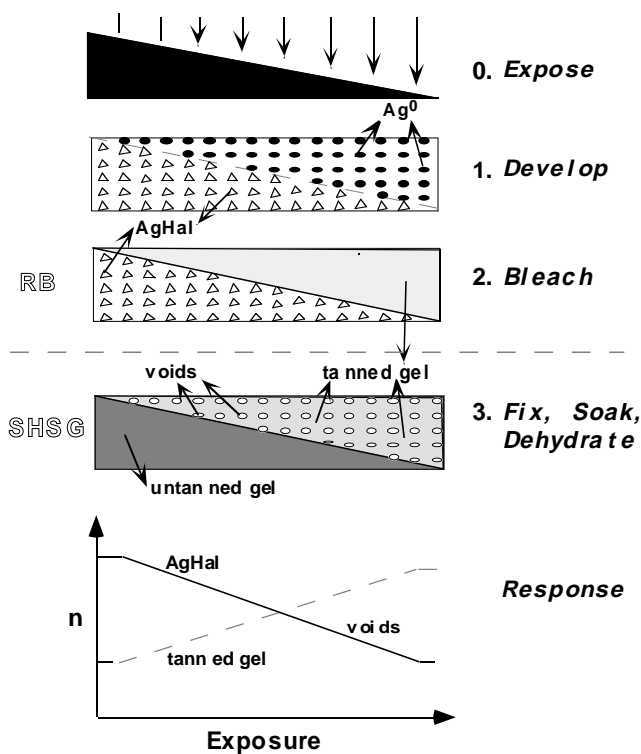


**Figure 2.** Schematic representation of the principal processing steps of RB and SHSG processing procedures in silver halide (AgHal) emulsions. The steps of RB are shown in the upper part of the figure; the steps of SHSG also include the lower part. The exposure responses of the refractive index are depicted for the individual contributions at the bottom.

than the unhardened ones. As a result, the DE of the holographically recorded patterns may increase or decrease depending on whether the refractive index versus exposure due to the AgHal grains changes in the same or opposite direction with that due to gelatin hardening.<sup>7,48</sup> As shown at the bottom of Fig. 2, the refractive index due to AgHal changes in the opposite direction to that of the gelatin hardening as would occur with the RB procedure. Note that with the direct bleach procedure, the changes would be in the same direction.

It is also possible to store the holographic patterns as a refractive index modulation primarily due to gelatin hardening.<sup>5,8,9,51</sup> In AgHal emulsions, this is achieved with the SHSG procedure, as shown in Fig. 2 (Steps 1 to 3). The initial difference in gelatin structure induced by differential hardening is amplified by the subsequent washing and dehydration steps. An additional<sup>1</sup> contribution to the refractive index modulation may be introduced in the SHSG procedure by gelatin matrix voids produced due to AgHal removal. The final sizes of the voids depend on the degree of gelatin hardening and swelling.<sup>9</sup> The refractive index of the voids is typically lower than that of gelatin so that the gelatin matrix voids change the refractive index in the opposite direction relative to that of the gelatin hardening.

**Experimental Procedures and Results.** Transmission holographic gratings were formed in AgHal commercial photographic plates by recording the interference pattern of two plane waves. The plane waves were derived from an argon laser at wavelength of 514 nm and were symmetrically incident on the plates. The RB processing procedures were evaluated with photographic plates (Agfa 8E56) and incident angles of  $\pm 30^\circ$ ; thus the recorded spatial frequency

was about 2000 lines/mm. The SHSG processing procedures were evaluated with photographic plates (Kodak 649F) and incident angles of  $\pm 15^\circ$ ; thus the recorded spatial frequency was about 1000 lines/mm. Reflection gratings were recorded with two plane waves: one incident from the emulsion side at  $+5^\circ$  and the other from the opposite substrate side at  $-15^\circ$ , resulting in a spatial frequency of about 3800 lines/mm. This configuration was chosen to separate between refracted and specularly reflected readout.

The DE was determined by reading out the powers of incident ( $I_i$ ), transmitted ( $I_t$ ), and diffracted ( $I_d$ ) beams at Bragg conditions. The absolute DE is then given by

$$DE = I_d/I_t \quad (11)$$

To correct for the losses from reflection, absorption, and scattering, the transmittance through the exposed and processed gratings far from the Bragg conditions were measured. Thus, the normalized and exposure-dependent DE is given by the ratios of the diffracted powers to the transmitted powers at normal incidence, as

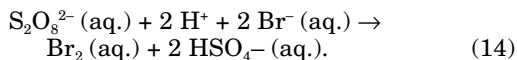
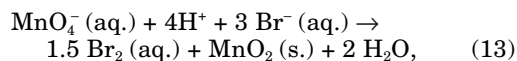
$$DE_{\text{norm}}(p) = I_d(p)/I_t(p)\cos\theta \quad (12)$$

To evaluate the long-term stability to read-out and environmental radiation, we used an accelerated light stability test: The processed holograms were illuminated with a laser beam set at an exposure energy of 100 J/cm<sup>2</sup> from an Ar laser at 514 nm; this exposure represents an increase of about 5 orders of magnitude relative to normal readout levels. In addition, the holograms were exposed to direct sunlight for several hours. The resultant photolytic darkening was measured with a spectrophotometer at 514 nm as the transmittance  $T_e$  of the exposed holograms and expressed as a change in optical density.<sup>7</sup>

The evaluated developers were CW-C2, which is a catechol-containing solution;<sup>43</sup> MAA, which is a metol-ascorbic acid developer formulation;<sup>7,48</sup> and MAAS, which is a newer, sulfite-containing version<sup>10</sup> of MAA. Both MAA and MAAS produce<sup>7,23</sup> a sensitivity increase by a factor of about 6 over CW-C2. The developer formulations are detailed in Table III.

The bleaches tested<sup>7</sup> contained either ammonium dichromate (ADC) with sulfuric acid (SA) or ferric sulfate (FS) as the oxidizer to which either potassium permanganate (KPM) or ammonium persulfate (APS) were added for the oxidative in vitro synthesis of bromine from potassium bromide (KBr). Some bleach formulations are detailed in Table IV.

The quantity of molecular bromine generated in the bleach solutions according to the spectroscopic analysis<sup>7,23</sup> together with the calculated stoichiometric quantities and solution redox potentials are listed in Table V. The transmittance  $T_u$  of unexposed and processed photographic plates (Agfa 8E56) as well as transmittance  $T_e$  after accelerated illumination are also included in Table V. The calculated bromine values for the bleaches WM-X1 (containing ADC, KBr, and KPM)<sup>7,23</sup> and WM-Y1, WM-Y3, or WM-F1 (Table IV) were determined according to the following chemical reactions, respectively:



In the reference bleach solutions ADC / SA / KBr (WM-Y0) and FS/KBr (WM-F0), no bromine could be detected;

**TABLE III. Developer formulations used in RB and SHSG Processing Procedures**

Chemical	CW-C2 (g/l)	MAA (g/l)	MAAS (g/l)
Catechol	10	—	—
Metol	—	2	2
Ascorbic acid	5	20	20
Urea	50	—	—
Sodium sulfite	5	—	50
Sodium carbonate (anhydrous)	30	50	50
Deionized water	to 1 l	to 1 l	to 1 l

**TABLE IV. Formulations of WM-X and WM-Y Bleaches**

Chemical <sup>a)</sup>	WM-Y0	WM-Y1	WM-Y2	WM-Y3	WM-F0	WM-F1
ADC	3	3	3	—	—	—
KBr	30	30	30	30	30	30
SA conc. (cc/l)	2	2	2	2	—	—
APS	—	10	—	10	—	10
FS	—	—	—	—	30	30
Br <sub>2</sub> (cc/l)	—	—	1.0	—	—	—
EDTA	—	—	—	—	30	30

a) Quantities in g/l, unless otherwise indicated, ADC—ammonium dichromate; SA—sulfuric acid; APS—ammonium persulfate; FS—ferric sulfate; EDTA—ethylene diamine tetraacetic acid disodium salt.

**TABLE V. Measured (anal.) and calculated (calc.) bromine concentrations, redox potentials (E) and holographic emulsion transmittance, unexposed (T<sub>u</sub>) and exposed by accelerated light stability test exposure (T<sub>e</sub>) S for different bleach formulations.**

Bleach	Br <sub>2</sub> (anal.) (cc/l)	Br <sub>2</sub> (calc.) (cc/l)	E (calc.) (V)	T <sub>u</sub> (%)	T <sub>e</sub> (%)
PBQ-2	—	—	—	67.7	40.5
WM-X0	—	—	—	62.0	42.0
WM-X1	0.9	1.0	+0.42	70.5	70.5
WM-X2	1.0	—	—	71.5	71.5
WM-Y0	—	—	-0.21	61.5	57.4
WM-Y1	0.3	0.8	+0.73	70.0	70.0
WM-Y2	1.2	—	—	71.1	71.1
WM-Y3	0.2	0.8	+0.94	69.4	68.6
WM-F0	—	—	-0.03	60.2	53.7
WM-F1	—	0.8	+0.91	68.6	67.8

this is consistent with the calculated negative redox potentials (see Table V) of these systems.

The absorption spectra of a holographic emulsion (Agfa 8E56), exposed and processed with WM-Y2, according to a reversal bleach procedure<sup>7,10,23</sup> clearly indicated that bromine is adsorbed into the holographic AgHal/gelatin coating. Furthermore, the disappearance of the charge transfer transition strongly suggested that bromine is mainly adsorbed at the AgHal interface.<sup>7,23</sup> We also found that photolytic darkening with our samples could occur after prolonged soaking in water and isopropanol with a concomitant disappearance of the bromine absorption bands.

Figure 3 shows the change in optical density (OD) induced by the accelerated illumination (exposure of 100 mJ/cm<sup>2</sup>) as a function of the holographic recording exposure for different bleach formulations. Clearly, the bleaches containing bromine (see Table V) show little, if any, deterioration in transmittance or OD after the accelerated light exposure. Not surprisingly, the bleaches with the highest bromine quantities (WM-X2, WM-Y2) also exhibited high stability at test conditions. Also evident is that relatively large density changes only occur with the bleaches not containing bromine. Moreover, these changes increase monotonically with exposure as shown in Fig. 3. This last observation is indicative of an increase in sensitivity to printout silver formation due to an increase in AgHal grain size<sup>20</sup> with recording exposure as a consequence of AgHal material transport during the bleaching process.<sup>12,23,24</sup> The same samples were also inert to direct sunlight exposure. Also no signs of darkening were found with samples over one year old that were processed with WM-X2; this indicates that long-term stability can be achieved with this bleach.

The absolute DE as a function of exposure for transmission gratings developed in CW-C2 and bleached with three different solutions according to a RB processing procedure<sup>7,10,23</sup> are depicted in Fig. 4. Two phenomena become apparent when comparing the two ADC / KPM (WM-X0, X1) based bleaches against a well-known parabeno-

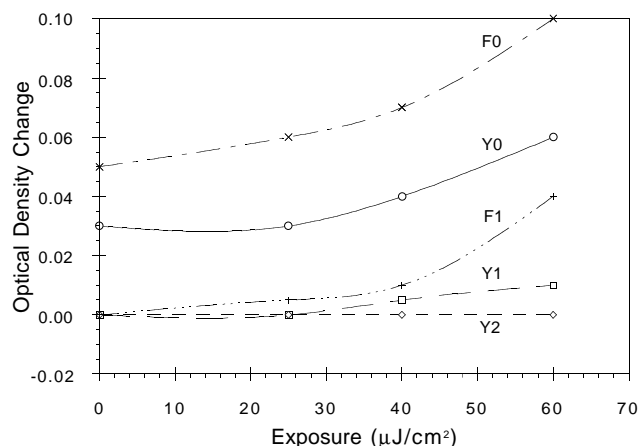


**Figure 3.** Change in optical density induced by accelerated illumination (100 J/cm<sup>2</sup>) as a function of recording exposure for different WM bleach formulations. The developer used was MAA.

quinone based bleach (PBQ-2).<sup>7,42,43</sup> First, the DE response is shifted to higher exposures and, second, the maximum DE reached are significantly higher with the KBr containing bleach (WM-X1). While the first mainly indicates a different refractive index modulation response, the second is also partly due to an increase in transmittance through the processed emulsion. This higher transmittance stems from bromine bleaching the sensitizing dye in the recording layer<sup>20</sup> as observed by the disappearance of the magenta coloration and the appearance of the yellowish emulsion color.

The bleaches containing bromine were also evaluated for reflection holographic recording: Figure 5 shows DE as a function of exposure for reflection gratings recorded in Agfa 8E56 processed with the WM-X1 (KPM containing) formulation as well as those processed with PBQ-2 according to a RB procedure.<sup>7,10,23</sup> Here, comparable DE

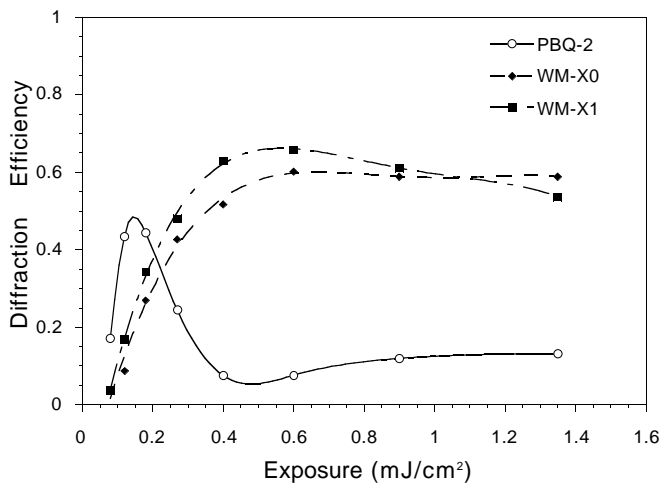


**Figure 4.** Diffraction efficiency as a function of exposure for holographic transmission gratings developed in CW-C2 and bleached with either PBQ-2, WM-X0, or WM-X1 formulations.

has been achieved by both bleach formulations; however, as discussed above, the new WM formulations were significantly more stable against photolytic darkening by print-out silver. No significant differences were found in the holographic results and the photolytic stability of emulsions processed in bleaches containing bromine that was either chemically synthesised in the bleach solution or added from the bottle and dissolved in the bleach.<sup>7,23</sup>

Our experimental results clearly indicate that bromine in the emulsion layer is the direct cause for the strong desensitization of photolytic print-out silver formation. In the presence of large quantities of  $\text{Br}_2$ , which is partly bound in the gelatin matrix and partly chemisorbed at the gelatin/AgHal interface, the inhibition of latent image formation can be explained by two mechanisms. First, from a molecular point of view, chemisorbed bromine dissociates into the atomic species and ultimately injects holes into the AgHal valence band,<sup>30</sup> which either increase recombination rates with electrons from the conduction band or reverse the nucleation process of metallic silver formation.<sup>20,30</sup> Second, from a thermodynamic point of view, the oxidation potential of the emulsion layer is significantly increased by the introduction of bromine, again causing heavy latent image inhibition.<sup>32</sup>

**The Holographic Storage Mechanism.** Based on experimental evidence, we have developed a relatively simple semiempirical model for elucidating the storage mechanism of bleached AgHal holograms.<sup>10</sup> The model treats the bleached emulsions as a composite material consisting of several components, all of which independently contribute to the overall refractive index modulation. These contributions are due to AgHal grains, gelatin, and gelatin matrix voids. The model predicts how each of these contributions may influence the DE versus exposure responses of holographic gratings recorded in bleached AgHal emulsions.<sup>10,23</sup>

For simplification, we assumed that the refractive index modulation owing to each of the three contributions of AgHal grains, gelatin hardening, or void formation are linearly dependent on exposure over a relatively large range. We believe this assumption to be valid, because the individual refractive index modulations result from secondary reactions of the silver halide development process;<sup>1</sup> such modulations have been determined to depend linearly on the silver optical density modulation,<sup>47</sup> which in turn

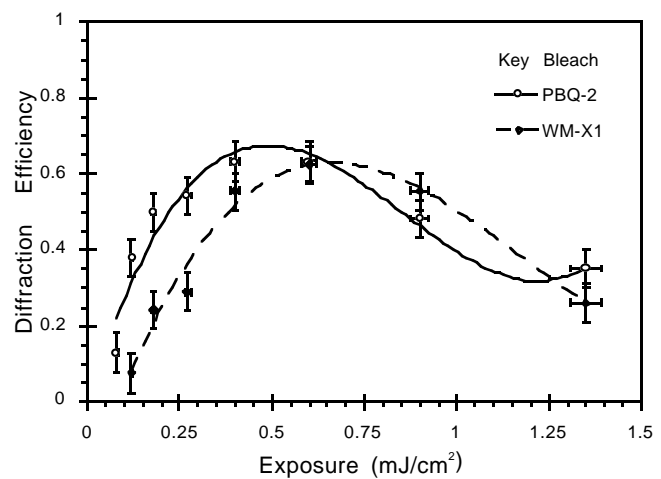


**Figure 5.** Diffraction efficiency as a function of exposure for holographic reflection gratings recorded in Agfa 8E56 and processed with the RB procedure; developed in CW-C2 and bleached with either PBQ-2 or WM-X1 formulations.

is essentially linear with exposure.<sup>1</sup> Such a linear dependence can be derived by the linear approximation of Eq. 6. The refractive index modulation at a given exposure can thus be derived from the difference between the refractive indices at some exposure level and zero exposure. Specifically, the linear dependence of the refractive index modulation on exposure  $p$  for any contribution  $i$  can now be written as

$$\Delta n_i(p) = \gamma_i p - t_i, \quad (15)$$

where  $\gamma_i$  and  $t_i$  are constants that depend on recording material properties as indicated in Eq. 6. The range for  $\Delta n_i(p)$  is  $0 \leq \Delta n_i(p) \leq \Delta n_{si}$ , where  $\Delta n_{si}$  is the refractive index change at saturation.

We can find the overall composite refractive index modulation as the sum of the modulations owing to the individual contributions by applying the Lorentz-Lorenz addition principle of fractional refractive indices for a multicomponent system<sup>24,44,50,52</sup> (Eq. 5), written as<sup>10,23</sup>

$$\Delta n_{tot}(p) = \sum_i \Delta n_i(p). \quad (16)$$

As alluded to in Fig. 2, there may be a phase shift of  $\pi$  between some of the contributions for certain processing procedures, such as RB. Such phase shifts of  $\pi$  are accounted for in Eqs. 9 and 16 by using the appropriate sign before  $\Delta n_i(p)$ . For example, for RB, the refractive index change with exposure owing to AgHal grains is negative, whereas that of gelatin is positive.

The three independent contributions have a total of nine independent variables as  $\gamma_i$ ,  $t_i$  and  $\Delta n_{si}$ . With the RB and SHSG processing procedures, only two contributions are dominant, and because the refractive index modulation owing to the individual contributions are interrelated with each other,<sup>7,8,9,20,49</sup> the number of independent variables can be reduced to three.<sup>10,23</sup> Substituting Eq. 15 into Eq. 16 and Eq. 16 into Eq. 10, which is the DE solution derived from the coupled wave theory,<sup>26</sup> yields the exposure-dependent diffraction efficiency for thick transmission phase gratings, with the grating vector being parallel to the recording plane, as

$$\eta(p) = A \sin^2 [\pi \Delta n_{tot}(p) L / 2 \lambda \cos \theta], \quad (17)$$

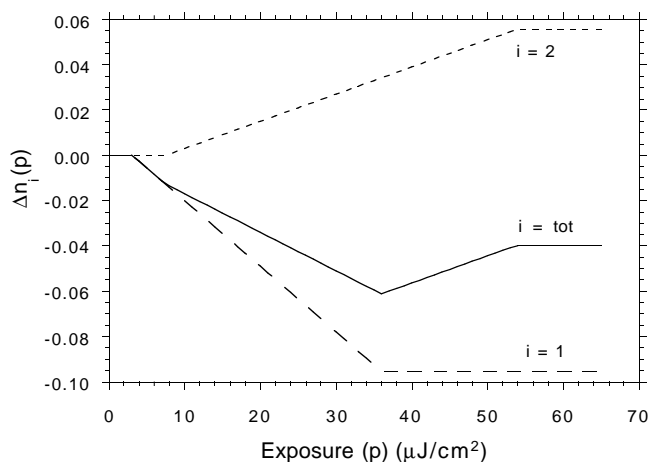


**Figure 6.** Refractive index modulation as a function of exposure in Agfa 8E56 emulsions, processed with the RB processing procedure. The linear responses of the AgHal ( $\Delta n_1$ ) and gelatin ( $\Delta n_2$ ) contributions with the parameters in Eq. 15 being  $\gamma_1 = -2.9 \times 10^{-3} \text{ cm}^2/\mu\text{J}$ ;  $\gamma_2 = 1.2 \times 10^{-3} \text{ cm}^2/\mu\text{J}$ ;  $t_1 = -t_2 = 0.9 \times 10^{-2}$ ;  $\Delta n_{s1} = -0.095$ ;  $\Delta n_{s2} = 0.055$ .  $\Delta n_{\text{tot}} = \Delta n_1 + \Delta n_2$ .

where  $A$  is the attenuation factor for absorption losses (equal to 1 for a pure phase material),  $L$  the grating thickness,  $\lambda$  the wavelength and  $\theta$  the incidence angle of the readout beam. The grating thickness  $L$  is assumed to be independent of exposure  $p$ . This assumption is reasonable for the RB and SHSG processing procedures. Specifically, with the RB procedure, we use a rehalogenating bleach formulation, in which there is almost no AgHal removal from the emulsion layer, and consequently almost no shrinkage. With the SHSG procedure,<sup>8,9,10,23</sup> the shrinkage that occurs by complete AgHal removal (fixing) is uniform and independent of exposure. However, with other processing procedures, such as in the direct bleach procedure, shrinkage is dependent on exposure,<sup>44</sup> and so  $L(p)$  must replace the constant  $L$  in Eq. 17.

Our model was evaluated by recording holographic gratings in bleached silver halide materials using the RB and SHSG processing procedures. Specifically, the RB procedure was tested to determine the influence of adding sulfite to a tanning developer formulation (MAA), and the SHSG procedure was tested to determine the influence of gelatin-swelling agents introduced into the hot water soak bath.

The linear responses of the refractive index modulation versus exposure for the individual contributions were determined separately by using interferometric knife edge experiments.<sup>10,23</sup> Figure 6 shows the experimental refractive index modulation as a function of exposure in Agfa 8E56 emulsions, which were processed with the RB processing procedure, using the MAA developer. The results shown are for two contributions in a composite emulsion system with linear responses according to Eq. 15. As can be seen, the slopes of the two contributions have opposite signs, which reflect their reversal ( $\pi$ -shifted) response; a negative slope was obtained for the response of the AgHal contribution ( $i = 1$ ) and a positive slope for the contribution due to gelatin tanning ( $i = 2$ ). Note that the resultant composite emulsion response goes through a minimum before reaching saturation.

Figure 7 presents the calculated and experimental DE versus exposure response for thick holographic transmission phase gratings recorded in Agfa 8E56 emulsions and processed with the RB processing procedure using the MAA

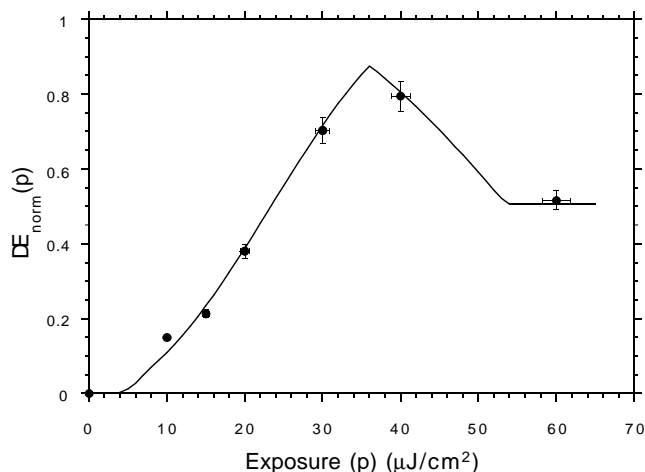
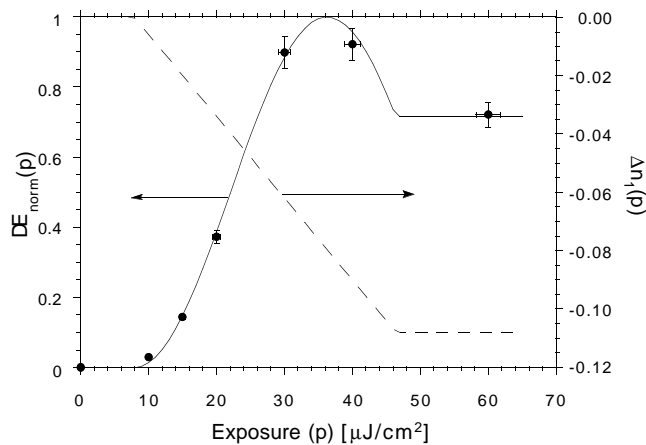


**Figure 7.** Calculated (solid line) and normalized experimental (points) DE as a function of exposure for holographic transmission gratings recorded in Agfa 8E56, developed in MAA, and bleached in WM-F1. The calculated DE response was computed according to Eq. 17, by using the composite refractive index modulation versus exposure response shown in Fig. 6. The constants in Eq. 17 were  $T = 5.6 \mu\text{m}$ ,  $\theta = 30^\circ$ , and  $\lambda = 0.514 \mu\text{m}$ .

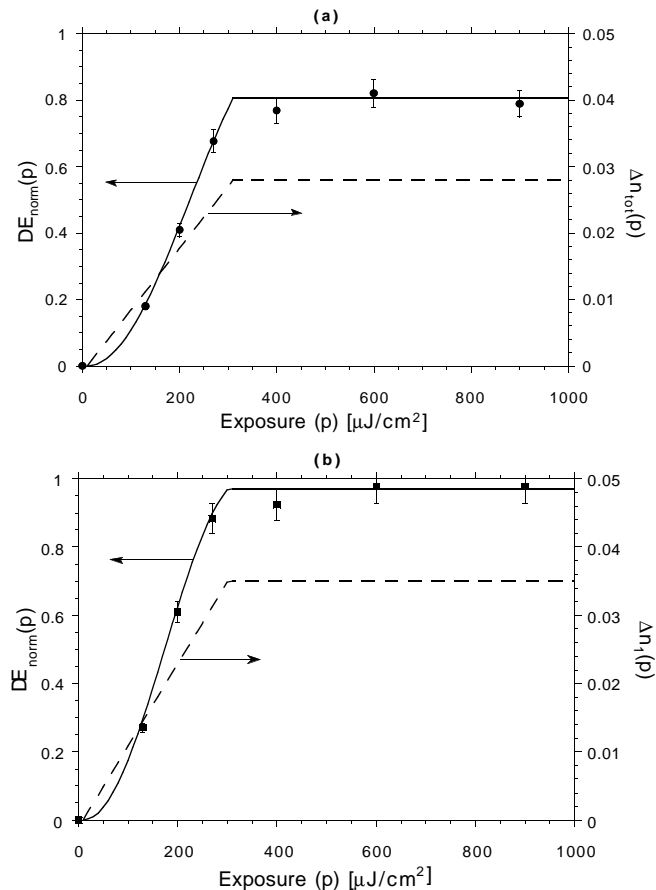
developer.<sup>7,10,23</sup> The DE response was calculated according to Eq. 17, by using the composite refractive index modulation versus exposure response shown in Fig. 6. The calculated response predicts a maximum DE of less than 100%; the maximum DE occurs where  $\Delta n_{\text{tot}}(p)$  is highest, indicating a limited dynamic range of the refractive index modulation of the composite emulsion. The good agreement between theory and experiment indicates that our model is indeed suitable for representing the holographic storage mechanism in reversal bleached emulsions. Specifically, the contribution owing to gelatin also has to be considered, especially when using a tanning developer formulation, such as MAA, even in conjunction with a nontanning bleach formulation, such as WM-F1.

Figure 8 depicts the calculated and experimental results for holographic transmission phase gratings recorded in Agfa 8E56 emulsions processed with the RB processing procedure using the MAAS developer.<sup>10,23</sup> These results, with the sulfite-containing formulation MAAS, show that the storage is primarily due to one contribution, i.e.,  $\gamma_2 = \Delta n_{s2} = 0$ , indicating that the gelatin matrix was not significantly affected by the MAAS processing. This is in agreement with the fact that the addition of a sufficient amount of sulfite to tanning developers suppresses the usual tanning action in combination with strongly oxidizing bleaches.<sup>49</sup> An important practical consequence of the elimination of the gelatin contribution, by processing with MAAS in the RB processing procedure, is that the maximal measured DE was increased by about 10% as seen by comparing Figs. 7 and 8. This was confirmed by the calculation predicting a maximum DE of 100% with only one contribution.

Similarly, the refractive index responses were obtained for Kodak 649F emulsions, which were processed with the SHSG processing procedure.<sup>8,9,10,23</sup> Note that with the SHSG processing procedure, the contribution of the AgHal grains to the composite refractive index modulation is completely eliminated by the fixing and subsequent water soaking steps. Nevertheless, these steps cause void formation by material removal and subsequent amplification by gelatin swelling (see Fig. 2). In any case, only two contributions need be considered. Because they originate from the initial silver development processing step, identical



**Figure 8.** Calculated (solid line) and normalized experimental (points) DE and refractive index modulation (dashed line) as a function of exposure for holographic transmission gratings recorded in Agfa 8E56, developed in MAAS, and bleached in WM-F1. The calculated DE response was computed according to Eq. 17 by using the refractive index modulation response shown, owing to AgHal only. The constants in Eq. 17 were  $T = 5.6 \mu\text{m}$ ,  $\theta = 30^\circ$  and  $\lambda = 0.514 \mu\text{m}$ ;  $\gamma_1 = -2.8 \times 10^{-3} \text{ cm}^2/\mu\text{J}$ ,  $t_1 = 2.2 \times 10^{-2}$ ,  $\Delta n_{s1} = -0.108$ .



**Figure 9.** Calculated (solid line) and normalized experimental (points) DE as a function of exposure for holographic transmission gratings in Kodak 649F, processed as SHSG. (a) The calculated DE response was computed according to Eq. 17, using the composite refractive index modulation versus exposure response (dashed line) and the constants  $T = 12.6 \mu\text{m}$ ,  $\theta = 15^\circ$ , and  $\lambda = 0.514 \mu\text{m}$ . (b) With TEA 10% in the hot water soak. The calculated DE response was computed according to Eq. 17, using the refractive index modulation response (dashed line), owing to gelatin tanning only with  $\gamma_1 = 1.2 \times 10^{-4} \text{ cm}^2/\mu\text{J}$ ;  $t_1 = -1.2 \times 10^{-3}$ ;  $\Delta n_{s1} = 0.035$ , as the parameters.

threshold and saturation exposure values were chosen. Linear responses according to Eq. 15 were taken for the individual contributions. A response with positive slope was obtained for the contribution owing to gelatin tanning ( $i = 1$ ) and a negative and much lower slope for the gelatin matrix void formation ( $i = 2$ ).<sup>10,23</sup>

The DE responses for holographic transmission gratings recorded in Kodak 649F are presented in Fig. 9. Figure 9(a) shows the calculated and experimental responses of DE as a function of exposure for holographic transmission gratings processed with the SHSG procedure.<sup>8,9,10,23</sup> The calculated DE response was computed according to Eq. 17, by using the composite refractive index modulation versus exposure response shown in Fig. 9(a). Good agreement exists between the calculated and experimental results. This verifies our assumption that the storage mechanism in SHSG holographic gratings essentially involves two contributions. Figure 9(b) depicts the response of the overall refractive index modulation, and the calculated and experimental DE as a function of exposure for transmission gratings processed with SHSG in the presence of triethanolamine (TEA).<sup>8,9,10,23</sup> The TEA was introduced into the hot water soak solution at 10%. Again, good agreement between the experimental and calculated results was obtained with only one contribution being dominant; in this case, the refractive index modulation is solely due to gelatin tanning. These results indicate that TEA influences the dynamic range of the composite refractive index modulation. This can be attributed to index matching or mismatching of voids in the gelatin matrix by gelatin-swelling agents.<sup>9</sup> Because TEA with a refractive index of about 1.47 is much closer to the gelatin refractive index ( $n \approx 1.50$ ) than the indices of other liquids involved in the processing, such as water ( $n = 1.33$ ) and isopropanol ( $n = 1.38$ ), the contribution owing to matrix void formation is negligibly small. Note that the experimental results with the swelling agent sorbitol ( $n \sim 1.33$ ) instead of TEA were identical within experimental error to the pure water soak control results.<sup>9</sup>

The close agreement between the calculated and experimental results in the linear region (below saturation) confirms the validity of our model. In the saturation region, the experimental results showed increasing deviations from the theoretical curve. This indicates that other factors are becoming increasingly important in the saturation region. These include recording nonlinearity,<sup>45,46</sup> recording intermodulation noise (noise gratings),<sup>47</sup> and increased grain size,<sup>7</sup> all leading to increased light scattering during readout<sup>46,50</sup> and decrease in dynamic range owing to increasing contribution of bias illumination.<sup>47</sup> Another effect not included in our model but that may become increasingly important at high exposures is the chemical neighbor effect, which contributes to nonlinear recording.<sup>20</sup>

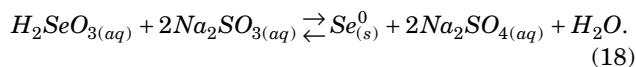
## Inorganic Colloids

**Photodeposition Processes and Mechanisms.** The formation of thin layers by photodeposition (PD) from inorganic colloid solutions irradiated by visible and ultraviolet radiation has been investigated since the late 1970s.<sup>11,53–57</sup> Specifically, photodeposition of amorphous selenium (a-Se) layers has been exploited for recording high-resolution patterns<sup>56</sup> and submicrometer holographic gratings.<sup>11,12,13</sup> The PD holograms are ultrathin surface relief gratings of layer thicknesses in the range of tens to hundreds of nanometers.<sup>11,12,13</sup> More recently, cadmium sulfide (CdS) or zinc sulfide (ZnS) colloids, irradiated with UV and visible light, were found to form similarly thin Cd or Zn layers.<sup>14,15</sup>

Photodeposition has the following inherent advantages: first, the deposited thin film thickness as well as lateral film thickness variations can be accurately controlled. Second, optical recording is carried out in one step without the need of additional chemical processing steps (such as in photolithography). The main disadvantage of the current colloidal PD systems is their low exposure sensitivity; e.g., to deposit a film of 100 nm thickness, an exposure of several J/cm<sup>2</sup> is needed.<sup>12-13</sup>

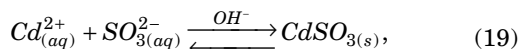
To explain the various processes involved in PD, let's resort to the schematic representation of Fig. 10. The photoreactor cell, filled with the colloidal solution, is irradiated through the transparent window. As a result of the irradiation, the following macroscopic photochemical/photophysical phenomena were observed in the a-Se system: (1) The size of the colloidal particles increased.<sup>53,54,58</sup> This leads to (2) sedimentation of the colloid to the bottom of the cell.<sup>53,54,58</sup> (3) solid a-Se material is photodeposited at the surface of the reactor window or on any other substrate immersed into the solution. With the recently developed CdS colloidal system,<sup>14</sup> additional phenomena have been observed: (4) An additional and different colloid of elementary Cd is formed in the reactor,<sup>14</sup> which may sedimentate, according to (2), and/or deposit,<sup>14</sup> according to (3). The phenomena associated with (1), (2), and (4) are called volume photoprecipitation (VP),<sup>14,53,54,58</sup> and those according to (3) are called surface photodeposition (SP).<sup>53,54</sup>

**Photodeposition Procedures and Results.** The preparation of the Se colloidal solutions are based on a slow chemical reduction of selenious acid in the presence of sulfite,<sup>53,54</sup> according to the reaction of

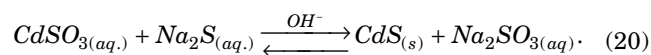


The detailed procedure to prepare the Se colloids includes three stages.<sup>53,54</sup> In stage (a) the cool reaction solution (4°C) is prepared; in stage (b), the nucleation and growth of solid a-Se particles, according to Eq. 18, is induced by heating the reaction solution (a) to room temperature, and, finally, in stage (c), the colloid solution of (b) is aged at 4°C for at least two days. The sizes of the particles at this stage range typically<sup>54,55</sup> from 10 to 70 nm. In order to obtain reproducible PD results, it is necessary to age the colloids, according to stage (c). When the colloids in the photoreactor cell (Fig. 10) are exposed to UV or visible radiation (<580 nm), the PD processes set in. The chemical transformation during PD can be described by an autocatalytic photoreduction reaction,<sup>58</sup> similarly to the dark reaction of Eq. 18.

The preparation of the photoactive CdS colloid sol is based on a two-step chemical reaction sequence of<sup>14</sup>



and



In the first step, a solution of a water soluble cadmium salt (CdCl<sub>2</sub>, Cd(NO<sub>3</sub>)<sub>2</sub>, etc.) is added to a solution of sodium sulfite producing solid cadmium sulfite as assessed by powder x-ray diffraction spectra and in accordance with Eq. 19. In the second step, the colloidal system is created

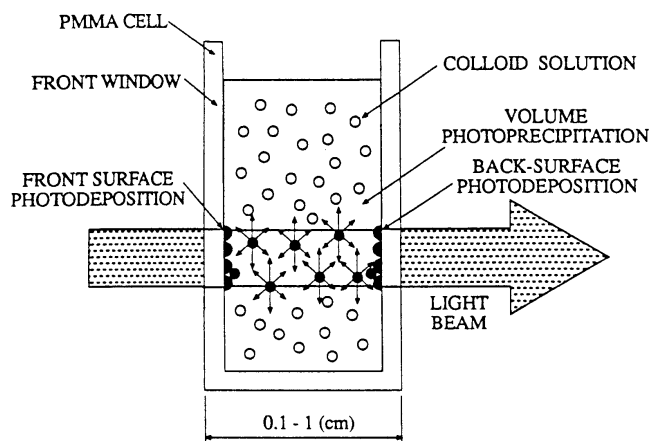


**Figure 10.** Schematic representation of a photoreactor cell and the volume photoprecipitation (VP) and surface PD (SP) processes.

by nucleation and growth of solid CdS particles, according to Eq. 20, by adding a solution of sodium sulfide to a solution containing the sulfites of cadmium and sodium. This two-step reaction sequence increases the exposure sensitivity of the colloid solutions by several orders of magnitude when compared to a one-step precipitation.<sup>14</sup>

For the PD experiments, the colloid solutions were poured into polymethylmethacrylate (PMMA) spectroscopic cuvettes of 1-cm optical path and equilibrated at the operating temperature. The metastability and photoactivity of the standard CdS hydrosol are shown in Fig. 11. It shows the effect of irradiation by a UV lamp (high pressure Hg with a power of about 1.6 W/cm<sup>2</sup>) on the colloidal absorption spectra.<sup>14</sup> The shoulder in the absorption spectra in the range of about 380 to 460 nm can be assigned to the CdS sol.<sup>59</sup> With irradiation, the absorption is significantly lower, indicating the decrease of CdS. This is owing to continuous transformation of CdS to Cd<sup>0</sup>, thereby gradually decreasing the number of CdS particles. As a consequence, the number of exposures that can be applied to the same sample is limited. Nevertheless, we found that by additional precipitation of CdS from the soluted Cd<sup>2+</sup> ions of irradiated sols (by adding Na<sub>2</sub>S, according to Eq. 20), their photoactivity could be recovered.<sup>14</sup>

As noted earlier, the exposure sensitivity of the CdS colloids increased significantly when a two-step reaction sequence, according to Eqs. 19 and 20, was used for the preparation. We attribute this sensitivity increase to the presence of cadmium sulphite that creates a reducing and basic environment enabling the photoreduction of CdS to elementary Cd<sup>0</sup>. This assumption is supported by further evidence: we found that the addition of sulfurous acid significantly decreased the exposure sensitivity and that the addition of hydroquinone or triethanolamine under basic conditions increased the exposure sensitivity.

The experimental results lead to three important conclusions.<sup>14,23</sup> First, the CdS colloidal particles are identified as the photoactive centers. Second, the number of CdS particles and not the soluted Cd<sup>2+</sup> concentration determine the photodynamic range. This represents an important difference between the CdS and the Se colloids where exhausting the Se colloid photoactivity is much more difficult, because additional Se particles are continuously generated during irradiation.<sup>53,58</sup> Third, basic and reducing conditions in the CdS colloid sol increase its photoactivity.

The temperature dependence of the film growth kinetics indicate that PD is not a pure photochemical process, but

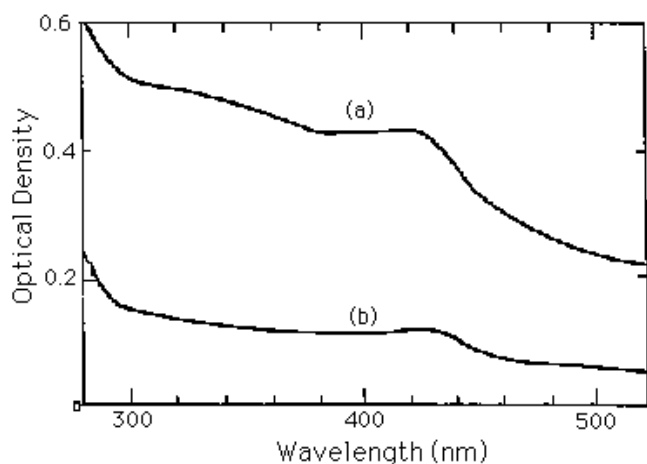


**Figure 11.** Absorption spectra of CdS colloidal sol. (a) nonirradiated; (b) irradiated sol with UV lamp beam of 1.6 W/cm<sup>2</sup>.

is governed by thermally activated processes. To estimate the magnitude of thermal activation of the SP process, the quasi-linear growth rates  $[d\xi/dt]_{QL}$  were determined at various temperatures<sup>14,23</sup> producing an Arrhenius-type activation graph shown in Fig. 12. In accordance to the Arrhenius-type activation equation of

$$[d\xi/dt]_{QL} = [d\xi/dt]_0 \exp(-E_A/kT), \quad (21)$$

we extract from the slope of Fig. 12 an activation energy of  $E_A \approx 0.68$  eV. From the similarity of the CdS activation energy to that obtained<sup>60</sup> for the Se PD process ( $E_A \approx 0.7$  eV), we assumed that the thermally activated processes involve chemical reduction of the photoactivated Cd<sup>2+</sup>/CdS to Cd<sup>0</sup>, Brownian motion of the colloidal particles from the bulk to the solution/substrate interface, and their adsorption onto the substrate.<sup>14,23</sup>

It was found that SP significantly depends on the substrate material as assessed from PD experiments with several substrate materials.<sup>14</sup> Specifically, the following relative substrate adsorption affinities were found for Cd:

$$\text{glass} < \text{mylar} < \text{PMMA} < \text{Cd film.}$$

It was therefore concluded that the colloidal particle adsorption onto the substrate represents the rate-determining step. This is also supported by the SP growth kinetics: the initial growth rates during the induction period are much smaller than those obtained during the continuation stage.<sup>14,54,61</sup>

We found that the exposure sensitivity decreased by several orders of magnitude when the irradiation wavelength was changed from the UV (364 nm) to the visible (458 nm).<sup>14,23</sup> Therefore, to determine the growth rates and deposition times of CdS sols at visible irradiation, we increased the sensitivity by resorting to reactor windows with predeposited thin Cd layers of about 200 Å. Figure 13 shows the Cd film deposition rates at two laser power levels as a function of photon energy derived from the discrete visible wavelengths of an argon laser. The deposition rates decrease as the laser power and wavelength increase. Note that the dependence of deposition rate on wavelength is much stronger than would have been expected from the spectral absorbance results (Fig. 11) alone.

Also remarkable is that the volume PD process (VP) disappeared at wavelengths above about 450 nm,<sup>14</sup> suggest-

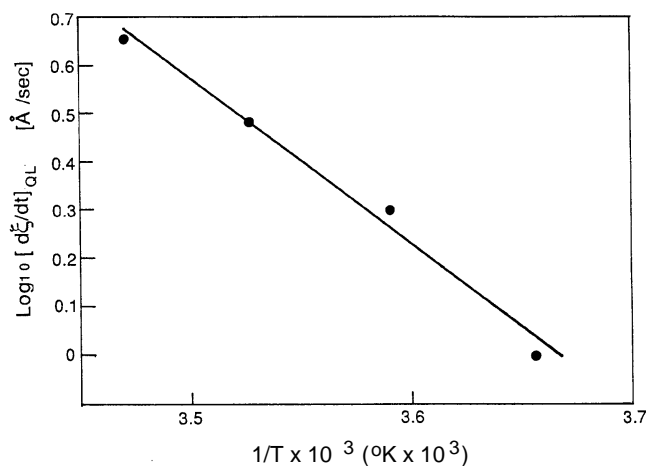


**Figure 12.** Log of quasi-linear Cd film growth rate as a function of the reciprocal photodeposition temperature.

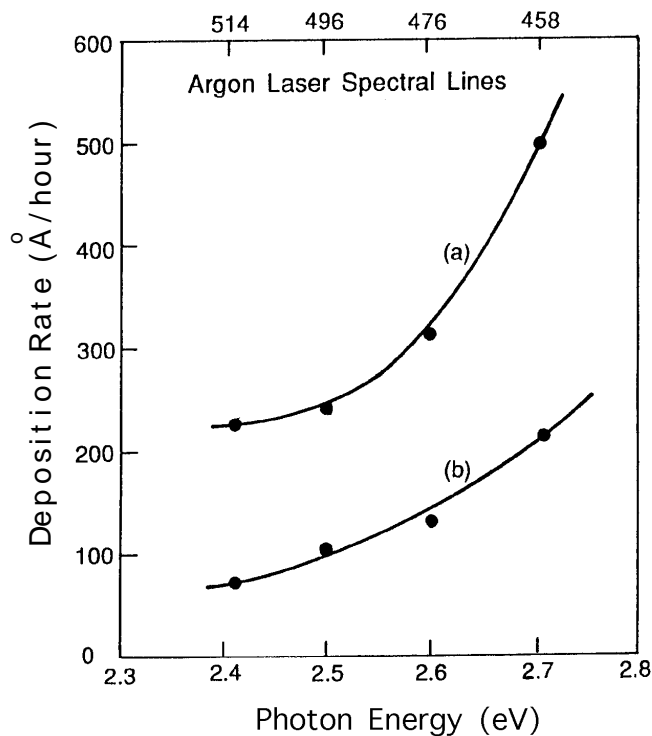
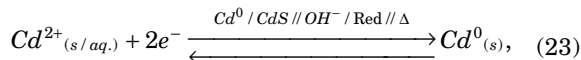
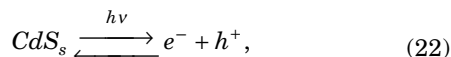


**Figure 13.** Cd film photodeposition rate as a function of photon energy (wavelength), at 22°C for various laser powers of (a) 10 W/cm<sup>2</sup>; (b) 7 W/cm<sup>2</sup>. Visible PD was on very thin predeposited Cd layers ( $\approx 200$  Å) on PMMA substrates.

ing that the PD process with CdS sols has to overcome an intrinsic threshold value of photon energy. From this transition to a pure SP deposition process (above about 450 nm), the threshold value is estimated at an energy of  $\geq 2.8$  eV. Similar evidence for an energy threshold mechanism was found for fluorescence excitation at wavelengths above 430 nm with CdS, confined in surfactant-containing colloids.<sup>59</sup> In the absence of VP, there is almost no scattering and the laser beam passes through the solution without attenuation. As a result, SP on predeposited windows, both in the front and the back of the reactor, proceeded at almost equal rates and layer thicknesses. These phenomena observed with the CdS system are the first direct experimental evidence that SP is a distinct step in the PD process.

A general PD model for our CdS colloids was proposed<sup>14,23</sup> that can consistently explain all the observed evidence. In this model, the chemical mechanism is best represented by the reaction scheme of



where Eq. 22 represents the primary step that by the absorption of light  $h\nu$  induces<sup>62</sup> the generation of electronic charge carriers ( $e^-$ ,  $h^+$ ) in the conduction and valence bands of CdS. Equation 23 schematically represents the secondary step that produces elementary cadmium ( $Cd^0$ ) and includes several subprocesses as alluded to by the symbols on top of the arrows:  $Cd^0/CdS$  indicates that the photogenerated electrons reduce CdS to  $Cd^0$ ; our investigations do not show whether this may result first in mesoscopic clusters within the CdS colloidal particles ( $Cd^0/CdS$ ) or whether these transform into elementary cadmium colloidal particles ( $Cd^0_{(s)}$ ) in one step. Either of these can occur according to the photon energy threshold evidence.  $OH^-/Red$  indicates that the  $Cd^0$  clusters/particles catalyze the fast chemical reduction of solid or soluted  $Cd^{2+}$  ions under basic ( $OH^-$ ) and reducing (Red) conditions. Similar catalytic behavior was observed with rhodium-coated CdS colloidal particles.<sup>62</sup> This subprocess may occur either with colloidal particles in the bulk solution (VP) or with particles adsorbed onto substrates (SP). The  $\Delta$  indicates that these subprocesses are temperature activated. As discussed earlier, SP differs from VP in that it must include an adsorption/desorption equilibrium during the initial deposition stage.

Note that the PD processes as described by Eqs. 22 and 23 exist as chemical equilibria, including the reverse processes of electronic carrier recombination<sup>62</sup> and the chemical oxidation ( $Ox$ ) of elementary cadmium to  $Cd^{2+}$  ions, respectively. These reverse processes are expected to decrease the quantum efficiency of the PD process. However, by choosing favorable chemical conditions ( $OH^-/Red$ ), carrier recombination can be reduced and the right arrow reactions increased as manifested by a significant increase in exposure sensitivities.<sup>14,23</sup>

**Holographic Photodeposition and Results.** Although, the precise mechanisms that govern the PD process are not completely clear yet, earlier investigations revealed that the processes leading to surface PD are highly localized;<sup>1-6</sup> they mainly occur in the irradiated areas of the interface between the solution and substrate, and the ultimate recording resolution seems to be related to the size of the colloid particles in the solution.<sup>55-57</sup> The following model<sup>12</sup> specifically accounts for holographic recording in conjunction with PD recording media. When recording simple holographic gratings by interference between two plane waves the cosinusoidal input exposure  $E_i$  along the  $x$ -direction is

$$E_i(x) = E_0 + E_1 \cos(2\pi x f), \quad (24)$$

where  $E_0$  is the average exposure,  $E_1$  is the amplitude of the modulated exposure, and  $f$  is the spatial frequency of the grating. The modulation function  $M_i$ , associated with this input exposure, is defined as  $M_i = E_i/E_0$ . Quite generally, the optical recording from colloids by PD is not linear

over wide exposure ranges.<sup>53,61</sup> However, a sufficiently large linear PD growth region exists over which the resultant thickness of the PD layer can be approximated by a linear exposure dependence.<sup>56,14</sup> In this linear range, the variation of the grown layer thickness along  $x$ , as a result of a cosinusoidal exposure  $E_i(x)$ , will be given by

$$h(x) = h_0 + h_1 \cos(2\pi x f), \quad (25)$$

where  $h_0$  is the average layer thickness and  $h_1$  is the amplitude of the film thickness variation. The corresponding surface grating modulation function  $M_g$  is then  $M_g = h_1/h_0$ . The modulation transfer function  $M$  of the photodeposited layer can be defined as the ratio of the modulation of the grating surface to the input exposure,<sup>29</sup> that depend on the spatial frequency of the exposure, hence:

$$M(f) = M_g(f)/M_i(f). \quad (26)$$

Alternatively, the modulation transfer function  $M(f)$  can be derived by considering how the optical input signal is affected by the colloidal recording medium. When recording a linear interference pattern, this can be described by a linespread function characteristic of the photodeposition recording material. The optical linespread function is the spatial intensity profile produced by a thin (input) sheet of light when scattered by the recording medium. Similar to photographic emulsions, the spatial linespread function  $A(x)$  can be written as<sup>63</sup>

$$A(x) = \frac{1}{K} e^{-2|x|/K}, \quad (27)$$

where  $K$  is the linespread parameter that depends on the characteristics of the recording material. The  $M(f)$  is obtained by taking the Fourier transform of the linespread function of Eq. 27, to yield<sup>63</sup>

$$M(f) = [1 + (\pi K f)^2]^{-1}. \quad (28)$$

To derive the  $M(f)$  in PD systems, the mechanisms that contribute to the linespread parameter  $K$  were considered. These included the optical extinction cross section<sup>58</sup> and linear particle aggregation number ( $N = 3$ ); the optical cross section included<sup>55,57</sup> the geometrical cross section of  $\pi a^2$  for monodisperse particle sizes  $a$ , and the correction factor  $n/\lambda_0$ , accounting for the light scattering cross section,<sup>64</sup> with  $n$  being the refractive index of the colloidal recording medium. Accordingly, the PD modulation transfer function was written as<sup>12</sup>

$$M(f) = [1 + (3\pi^2 n a^2 f / \lambda_0)^2]^{-1}. \quad (29)$$

Because in our experiments we also measured the frequency response of the diffraction efficiency, we have to relate it to the theoretical  $M(f)$  derived in Eq. 29. For thin phase holographic gratings used in our investigations, the diffraction efficiency is given by<sup>11,13</sup>

$$\eta(f) = \frac{1}{4} (2\pi \Delta n h_1(f) / \lambda_0)^2, \quad (30)$$

where  $\Delta n$  is the difference between the refractive indices of the grating and the surrounding medium (air) and  $\lambda_0$  is the freespace readout wavelength. Using Eqs. 26 and 30, we obtain another theoretical expression for the  $M(f)$  response in our thin phase holographic grating system:

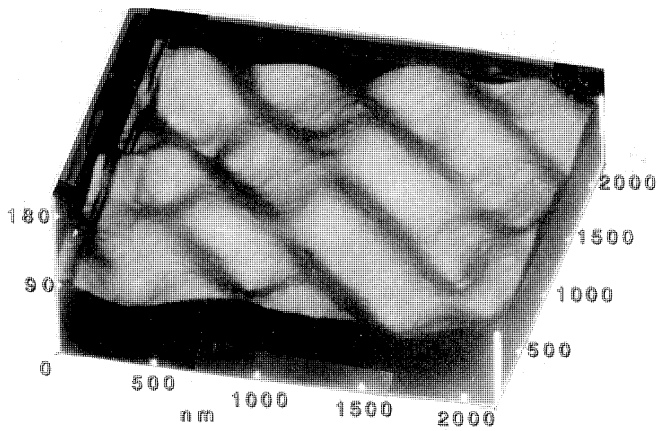


**Figure 14.** AFM micrograph of a holographic grating recorded by PD from an a-Se sol.

$$M(f) = \frac{\lambda_0 \eta^{1/2}(f)}{\pi \Delta n h_0 M_i} \quad (31)$$

Finally, from Eqs. 29 and 31, we obtain the frequency response of the diffraction efficiency for photodeposited gratings:

$$\eta^{1/2}(f) = \frac{\pi \Delta n h_0 M_i / \lambda_0}{1 + (3\pi^2 n a^2 f / \lambda_0)^2} \quad (32)$$

To conclude the theoretical section above, we observe that Eq. 29 relates the frequency response of the modulation transfer function to the microscopic parameters of the colloid system. Similarly, Eq. 32 relates the theoretical diffraction efficiency frequency response to the microscopic characteristics of the colloid.

For holographic recording,<sup>11,12</sup> the colloid solutions were first equilibrated at room temperature and poured into polymethylmethacrylate (PMMA) spectroscopic cuvettes. For simplicity, the cuvettes were not temperature controlled; such control would be necessary, however, if high reproducibility of results is desired. Nevertheless, this is of little importance when evaluating normalized results that correct for eventual temperature fluctuations and, as a result, thickness variations. The colloid solutions in the PMMA cuvettes were then illuminated by the interference patterns of two plane waves from an Ar ion laser at wavelengths of 488 and 514 nm and exposures ranging from 3 to 1000 J/cm<sup>2</sup>. The offset angle between the two beams was varied between 20° and 70° to obtain spatial frequencies ranging from about 700 to about 2200 lines/mm. As a result, a-Se gratings were photodeposited on the front and back surfaces in accordance with the process given in Eq. 18. The optical readout of the holographic gratings was performed with an He-Ne laser at 633 nm; this wavelength was chosen so that the transmission through the a-Se films would be larger.

The grating morphology was determined by two independent methods;<sup>13</sup> atomic force microscopy (AFM),<sup>13,23</sup> and optical readout. The AFM micrograph in Fig. 14 shows an area of 2000 × 2000 nm of a typical PD hologram with a grating period of about 500 nm. The cosinusoidal surface relief is of relatively smooth texture indicating that the colloidal particles coalesce during the PD film growth.<sup>57</sup> Alternatively, from the measured DE, we evaluated<sup>11,12</sup> the

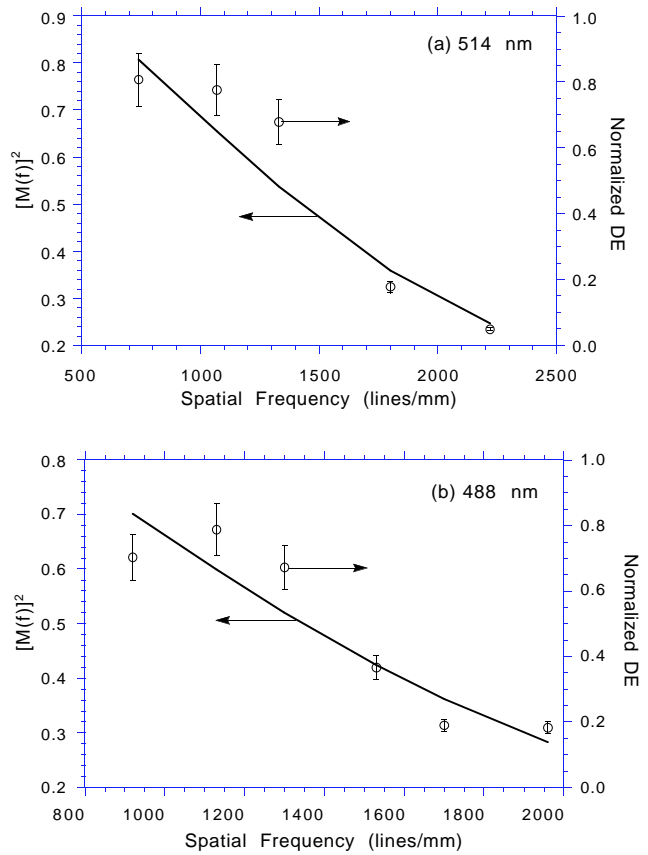


**Figure 15.** Theoretical  $[M(f)]^2$  (solid line) and experimental DE (points) as a function of spatial frequency for PD holographic gratings with recording wavelengths of (a) 514 and (b) 488 nm. The experimental points are normalized by the low-frequency values. The solid curves were calculated from Eq. 29 with  $n = 1.33$  and  $a = 77$  nm.

amplitudes of the film thickness variations  $h_1$ , according to Eq. 30. The resultant PD holograms were ultrathin surface relief gratings of average layer thicknesses in the range of 100 to 2200 nm and with amplitudes of the relief thickness variations in the range of 20 to 40 nm. Noteworthy is that the gratings recorded at  $\lambda = 488$  nm exhibited about twice the maximum DE than those recorded at  $\lambda = 514$  nm, i.e., 13% as compared to 6%. This is probably because the deposition rate at the wavelength of 488 nm is significantly greater than at 514 nm, allowing a faster grating recording time. Specifically, the PD exposure sensitivity of the gratings recorded at 488 nm was about 23 nm/J, and that at 514 nm was about 2 nm/J.

Figure 15 shows the experimental DE and theoretical  $M(f)$  as a function of spatial frequency for PD holographic gratings. The significant decrease of DE higher than 1300 lines/mm indicates that the resolution is limited in our a-Se colloid system. Equation 31 shows that  $M(f)$  is directly proportional to  $\eta^{1/2}$ ; therefore, in Fig. 15 the theoretical  $[M(f)]^2$  and the normalized experimental DE are compared. We observe that although the general tendency of the experimental points and the solid theoretical curves follow a similar behavior, some discrepancies occur. This indicates that our simplified model should include additional mechanisms. For example, in our model, Brownian motion of the particles and ionic diffusion were neglected.<sup>12</sup> Also, ionic diffusion between the irradiated and dark areas at the substrate/solution interface with increasing spatial frequency should

be included. Such adjacency effects have been observed and accounted for in the responses of modulation transfer functions in photographic emulsions.<sup>63</sup>

The theoretical frequency response in Fig. 15 was calculated from Eq. 29 for particles with sizes of 77 nm. Because the experimental holographic gratings were photodeposited with colloidal particles of sizes ranging from 30 to 80 nm, the results indicate that the recording resolution may be limited by the largest particles in the colloid population. Therefore, the colloid particle size distribution must be reduced to record higher spatial frequencies. For example, to exceed  $f \approx 3000$  lines/mm, it would be necessary to resort to particles with  $a_{\max} \leq 30$  nm.

## Conclusions

Inorganic material systems suitable for archival optical holographic recording were investigated, with an emphasis on bleached silver halide emulsions and colloidal solutions. Holographic recording and readout was shown to be a powerful tool for elucidating basic photochemical and photophysical mechanisms. Specifically, holographic recording helped to determine dispersive contributions to optical storage in composite phase recording materials. Also the microscopic deposition mechanism of inorganic colloidal particles could be evaluated by the spatial frequency response of holographic recording.

Bleached silver halide holograms generally suffer from photolytic degradation. By using bromine in the bleach bath formulations, significant increases in the image stability to photolytic degradation were found. The spectroscopic and holographic investigations indicated that  $\text{Br}_2$  is adsorbed onto the AgHal grains, which explains the increased stability by the inhibition of latent image formation and, consequently, of photolytic silver formation.

Experimental and theoretical investigations allowed us to differentiate between individual contributions to the refractive index modulation within the composite AgHal emulsion system. These contributions originate from microstructure formation induced by holographic recording and chemical processing, including silver halide grain reallocation by recrystallization and gelatin/gelatin void matrix structuring by crosslinking and swelling. Specifically, increased contribution from the gelatin matrix was found with tanning developer formulations, which include catechol or metol, and/or tanning bleach formulations, which include parabenzquinone or ammonium dichromate. But, reduced gelatin matrix contribution was found with the addition of sulfite to tanning developers and/or using nontanning oxidizing agents, such as ferric sulfate, in the bleach formulations and/or adding bromine to the bleach formulations. Furthermore, increased contribution of voids in the gelatin matrix was found in SHSG holograms with increased processing temperature. This contribution was reduced by the addition of triethanolamine to the water soak by index matching of the voids to the matrix.

The holographic experiments together with our theoretical analysis further revealed that the reduction in the number of contributions to the refractive index modulation in a composite emulsion layer may have a favorable practical consequence; namely, the maximum DE increases and may reach 100% in the case of homogeneous and lossless volume phase gratings. Note, however, that with composite systems, the dynamic range of refractive index modulation will only be limited if the slopes of individual contribution responses are of opposite signs.

The improvements achieved with our processing procedures and formulations of bleached AgHal emulsions in

terms of DE, SNR, and stability to readout and environmental radiation can be exploited for a number of holographic applications. These include holographic optical elements for replacing conventional refractive optics,<sup>9,65-67</sup> filters for optical pattern recognition,<sup>68,69</sup> elements for all-optical neural networks,<sup>70</sup> and planar holograms for three-dimensional display applications.<sup>71</sup> With planar holograms where the readout beam propagates within the holographic plate, losses due to light scattering become important. Therefore, we suggest further optimization of the present reversal bleach procedures to minimize grain growth during processing.

Inorganic colloidal solutions such as amorphous Se, CdS, and ZnS are deposited on substrates when irradiated with UV and visible radiation. The experimental evidence regarding photodeposition with the recently developed CdS colloidal system can be consistently explained by a relatively simple reaction model. The model shows several subprocesses similar to the Se system that seem, therefore, to be of general nature common to all colloidal PD systems. First, the colloidal particles are the photoactive centers that absorb the light and induce the primary photoelectronic charge generation. Second, the photoactivated colloidal particles then induce secondary processes, of which the most important one is chemical reduction under suitable (basic) conditions. In the bulk of the photoreactor, this leads to the particle growth and sedimentation of the sol, termed volume photodeposition (VP). Third, some colloidal particles move by Brownian motion to the solution/window interface, where they are adsorbed; the adsorption affinity depends on the substrate material. Similar to VP, the adsorbed and photoactivated particles again form chemically reduced material, which, in this case, results in the formation of thin films, termed surface photodeposition (SP). The SP process is thermally activated and is rate-limited by the adsorption step.

In addition, our results reveal some specific features that characterize certain colloidal systems. For example, the Se system consists of elementary particles, whereas the CdS particles are ionic solids. Therefore, the Se colloids photoreduce soluted  $\text{Se}^{4+}$  to solid  $\text{Se}^0$  by an autocatalytic process, keeping the same colloidal composition. This is different for the CdS sols, which photoreduce to  $\text{Cd}^0$  by a heterocatalytic process, thereby changing colloidal composition. In this respect, we may anticipate that, for example, Si or Ge colloidal systems would behave similar to the Se sols and that CdSe or AgBr colloid solutions would resemble the CdS system. Also interesting is the exposure response of the CdS system, which shows a much stronger dependency on wavelength than expected from the colloidal absorption spectra alone. This indicates a photon energy threshold barrier in the primary photoprocess mechanism. The threshold energy value is estimated to be about 2.8 eV as indicated by the absence of the VP process at wavelengths higher than 450 nm, where the SP process was performed onto predeposited Cd layers. This last phenomenon represents the first direct experimental evidence that SP is a distinct step in the PD process.

The resolution capabilities of the photodeposition process from inorganic colloids were analyzed by a theoretical model and determined experimentally by holographic recording. The proposed microscopic model relates the spatial frequency responses to optical recording parameters and to the colloid system particle sizes. Therefore, on one hand, the theoretical relationships enable us to evaluate the influence of colloid particle sizes on the resolution possible with the photodeposition process. On the

other hand, holographic recording can be exploited as an experimental method for determining the particle sizes of a given colloid from the measured resolution capabilities. The maximum experimental diffraction efficiency of holographic gratings recorded by photodeposition with a-Se colloids reached 13% with a spatial frequency of  $f = 1100$  lines/mm. The diffraction efficiencies decreased with increasing spatial frequency, and dropped to half of the maximal DE at  $f \approx 1500$  lines/mm. These resolution capabilities were achieved with colloid particle sizes reaching 80 nm. To obtain ultrahigh spatial frequencies of higher than 10,000 lines/mm, the theoretical derivation indicates that the colloid particle size should be restricted to  $a_{\max} \leq 10$  nm. ▲

**Acknowledgments.** The authors wish to express their gratitude to E. Millul, Y. Krivi, and A. Shalgi for their experimental assistance. These investigations were supported in part by the Israel Ministry of Science and Technology.

## References

- R. J. Collier, C. B. Burckhardt and L. H. Lin, *Optical Holography*, Academic Press, New York, Chaps. 10 and 12, 1971.
- Holographic Recording Materials*, H. M. Smith, Ed., Springer-Verlag, Berlin, 1977.
- Handbook of Optical Holography*, H. J. Caulfield, Ed., Academic Press, Chaps. 8 and 9, 1979.
- L. Solymar and D. J. Cooke, *Volume Holography and Volume Gratings*, Academic Press, New York, Chap. 10, 1981.
- P. Hariharan, *Optical Holography*, Cambridge University Press, Chap. 7, 1984.
- V. Weiss, A. A. Friesem, and V. A. Krongauz, Organic materials for real-time holographic recording, *J. Imaging Sci. Technol.* (1997).
- V. Weiss, E. Millul and A. A. Friesem, Photolytically stable bleached holographic silver images, *J. Imag. Sci. & Technol.* **37**(1), 92 (1993).
- V. Weiss and E. Millul, Bleached silver halide holographic recording materials, in *Holography Techniques and Applications*, Proc. SPIE **1026**, 55 (1988).
- V. Weiss, Y. Amitai, A. A. Friesem and E. Millul, Silver halide sensitized gelatin holographic recording materials, in *6th Meeting in Israel on Optical Engineering*, Proc. SPIE **1038**, 110 (1989).
- V. Weiss and A. A. Friesem, Storage mechanism of holograms in bleached silver halide emulsions, *J. Opt. Soc. Am. A* **11**, 2004 (1994).
- A. Peled, V. Weiss, D. Rosenblatt and A. A. Friesem, Holographic recording by photodeposition techniques, *Opt. Eng.* **31**, 70 (1992).
- V. Weiss, A. Peled and A. A. Friesem, Spatial frequency response of holographic gratings photodeposited from inorganic colloids, *Appl. Opt.* **33**, 4988 (1994).
- A. Peled, V. Weiss, A. Shalgi and A. A. Friesem, Resolution capabilities of photodeposited holographic gratings, *Appl. Surf. Sci.* **79/80**, 393 (1994).
- V. Weiss, A. A. Friesem and A. Peled, Photodeposition of thin Cd films from CdS colloid solutions, *Thin Solid Films* **218**, 193 (1992).
- A. Peled, B. Dragnea, R. Alexandrescu and A. Andrei, Laser induced photodeposition from ZnS colloid solutions, *Appl. Surf. Sci.* **86**, 538 (1995).
- M. D. Fayer, Dynamics of molecules in condensed phases: Picosecond holographic grating experiments, in *Ann. Rev. Phys. Chem.*, **33**, 63 (1982).
- C. Brauchle and D. M. Burland, Holographic methods for the investigation of photochemical and photophysical properties of molecules, *Angew. Chem. Int. Ed. Engl.* **22**, 582 (1983).
- J. G. Calvert and J. N. Pitts Jr., *Photochemistry*, John Wiley & Sons, New York, 1966.
- K. I. Jacobson and R. E. Jacobson, *Imaging Systems*, The Focal Press, London, 1976, Chap. 1.
- T. H. James, in *The Theory of the Photographic Process*, Macmillan Publishing, 4th ed., 1977.
- R. C. Bertelson, in *Photochromism*, G. H. Brown, Ed., Wiley-Interscience, 1971, Chaps. III and X.
- Photochromism, Molecules and Systems*, Elsevier, H. Durr and H. Bouas-Laurant, Eds., 1990, Chaps. 2, 8, 10, 23 and 24.
- V. Weiss, *Photoactive Materials for Recording and Modulation of Optical Signals*, Thesis, The Weizmann Institute of Science, Rehovot, Israel, 1994.
- W. J. Tomlinson and E. A. Chandross, Organic photochemical refractive-index image recording systems, in *Advances in Photochemistry*, **12**, John Wiley & Sons, New York, 1980, p. 201.
- F. W. Deeg, J. Pinski, C. Brauchle and J. Voitlander, The evaluation of photochemical quantum yields by holography, *J. Chem. Phys.* **79**, 1229 (1983).
- H. Kogelnik, Coupled wave theory for thick hologram gratings, *Bell. Sys. Tech. J.* **48**, 2909 (1969).
- H. Hervet, W. Urbach and F. Rondelez, Mass diffusion measurements in liquid crystals by a novel optical method, *J. Chem. Phys.* **68**, 2725–2729 (1978).
- M. Gehrtz, J. Pinski and C. Brauchle, *Appl. Phys. B* **43**, 61 (1987).
- J. W. Goodman, *Introduction to Fourier Optics*, McGraw-Hill, San Francisco, 1988 Chap. 7, pp. 157–160.
- J. F. Hamilton, The silver halide photographic process, *Adv. Phys.* **37**, 359 (1988) and literature cited therein.
- A. Hoffman, *Thermodynamic Theory of Latent Image Formation*, Focal Press/Butterworth 1982 and literature cited therein.
- A. Hoffman and V. Weiss, Recording, amplification and discrimination in silver halide imaging, *J. Photogr. Sci.* **39**, 220 (1991).
- R. W. Gurney and N.F. Mott, The theory of the photolysis of silver bromide and the photographic latent image, *Proc. Royal Soc.* **164a**, 151 (1938).
- D. H. McMahon and W. T. Maloney, Measurements of the stability of bleached photographic phase holograms, *Appl. Opt.* **9**, 1363 (1970).
- C. B. Buckhardt and E. T. Docherty, A bleach process for high-efficiency low noise holograms, *Appl. Opt.* **8**, 2479 (1969).
- P. Hariharan and C. S. Ramanathan, Suppression of printout effects in photographic phase holograms, *Appl. Opt.* **10**, 2197 (1971).
- M. Chang and N. George, Holographic dielectric grating: theory and practice, *Appl. Opt.* **2**, 713 (1970).
- H. T. Buschmann, Bleichprozesse zur Erzeugung rauscharmer lichtstarker Phasenhologramme, *Optik* **34**, 240 (1971).
- M. Lehmann, J. P. Lauer and J. W. Goodman, High efficiency, low noise and suppression of photochromic effects in bleached silver halide holography, *Appl. Opt.* **2**, 1948 (1970).
- H. Thiry, New technique of bleaching photographic emulsions and its application to holography, *Appl. Opt.* **11**, 1652 (1972).
- A. Graube, "Advances in bleaching methods for photographically recorded holograms," *Appl. Opt.* **13**, 2942 (1974).
- N. J. Phillips, A. A. Ward, R. Cullen and D. Porter, Advances in holographic bleaches, *Photogr. Sci. Eng.* **24**, 120 (1980).
- D. J. Cooke and A. A. Ward, Reflection-hologram processing for high efficiency in silver-halide emulsions, *Appl. Opt.* **23**, 934 (1984).
- R. L. van Renesse and F. A. J. Bouts, Efficiency of bleaching agents for holography, *Optik* **38**, 156 (1973).
- A. A. Friesem and J. S. Zelenka, Effects of film non-linearities in holography, *Appl. Opt.* **6**, 1755 (1967).
- C. W. Slinger, R. R. A. Syms and L. Solymar, Nonlinear recording in silver halide planar volume holograms, *Appl. Phys. B* **36**, 217 (1985).
- A. A. Ward and L. Solymar, Diffraction efficiency limitations of holograms recorded in silver-halide emulsions, *Appl. Opt.* **28**, 1850 (1989).
- P. Hariharan, Basic processes involved in the production of bleached holograms, *J. Photogr. Sci.* **38**, 76 (1990).
- A. G. Tull, Tanning development and its application to dye transfer images, *J. Photogr. Sci.* **11**, 1 (1963).
- R. L. van Renesse, Scattering properties of fine-grained bleached emulsions, *Photogr. Sci. Eng.* **24**, 114 (1980).
- D. Angell, Improved diffraction efficiency of silver halide (Sensitized) gelatin, *Appl. Opt.* **26**, 4692 (1987).
- W. J. Tomlinson, E. A. Chandross, H. P. Weber and G. D. Aumiler, Multicomponent photopolymer systems for volume phase holograms and grating devices, *Appl. Opt.* **15**, 534 (1976).
- M. Perakh and A. Peled, Photodeposition of a Se Films by the Selor process, *Thin Sol. Films* **50**, 273 (1978); *ibid.*, **50**, 283 (1978); *ibid.*, **50**, 293 (1978).
- A. Peled, Development of a new process—photodeposition for producing thin films of amorphous selenium and investigation of their basic properties, *Ph. D. Thesis*, The Hebrew University, Jerusalem, July 1978.
- A. Peled, Studies of a-Se dispersions used in the photodeposition process: dispersion properties in the dark, *J. Dispersion Sci. Technol.* **5**, 219 (1984).
- A. Peled and Y. Dror, Optical imaging by the surface photodeposition effect, *Opt. Eng.* **27**, 482 (1988).
- A. Peled, Transformation steps of microstructures in photodeposited films of a-Se, *J. Mater. Res.* **27**, 177 (1989).
- A. Peled, Volume photodeposition process in a-Se hydrosols, *Colloid. Polym. Sci.* **262**, 817 (1984).
- Y.-M. Tricot and J. H. Fendler, In situ generated colloidal semiconductor CdS particles in dihexadecyl phosphate vesicles: Quantum size and asymmetric effects, *J. Phys. Chem.* **90**, 3369 (1986).
- A. Peled, D. Naot and M. Perakh, On the theory of photoadsorption kinetics of a-Se colloids, *Colloid Polym. Sci.* **266**, 958 (1988).
- A. Peled, A. A. Friesem and K. Vinokur, Continuous-wave laser photodeposition of amorphous selenium films, *Thin. Sol. Films* **218**, 201 (1992).

62. Y. M. Tricot and J. H. Fendler, Colloidal catalyst coated semiconductors in surfactant vesicles: In situ generation of Rh-coated CdS particles in dihexadecyl phosphate vesicles and their utilization for photosensitized charge separation and hydrogen generation, *J. Am. Chem. Soc.* **106**, 7359 (1984).
63. M. A. Kriss, *Image Structure*, in *Theory of the Photographic Process*, 4th ed., T. H. James, Ed. (McMillan, New York, 1977), Chap. 21, pp. 592–614.
64. H. C. van de Hulst, *Light Scattering by Small Particles*, Dover Publications, New York, 1981, Chap. 9, p. 128.
65. Y. Amitai, A. A. Friesem and V. Weiss, New designs of holographic helmet displays, in *Holographic optics: Design and applications*, *Proceedings SPIE* **883**, 12 (1988).
66. Y. Amitai, A. A. Friesem and V. Weiss, Holographic elements with high efficiency and low aberrations for helmet displays, *Appl. Optics* **28**, 3405 (1989).
67. Y. Amitai, A. A. Friesem and V. Weiss, Designing holographic lenses with different recording and readout wavelengths, *J. Opt. Soc. Am. A* **7**, 80 (1990).
68. I. Glaser, M. Cohen, V. Weiss, H. Bernstein and A. A. Friesem, Pattern recognition with incoherent holographic correlators, in *Optics and the Information Age*, *Proc. SPIE* **8**, 13 (1987).
69. S. Gorodeisky, M. Cohen, A. A. Friesem, I. Glaser and V. Weiss, Holographic correlator with multiple model filters, in *6th Meeting in Israel on Optical Engineering*, *Proc. SPIE* **1038**, 168 (1989).
70. I. Shariv, T. Grossman, E. Domany and A. A. Friesem, All-optical implementation of the inverted neural network model, *Proc. SPIE* **1319**, 194 (1990).
71. Y. Amitai et al., White-light holographic display based on planar optics, *Opt. Lett.* **8**, 1265 (1993).